

Article

Physiologically Based Pharmacokinetic Modelling to Predict Pharmacokinetics of Enavogliflozin, a Sodium-Dependent Glucose Transporter 2 Inhibitor, in Humans

Min-Soo Kim ^{1,†}, Yoo-Kyung Song ^{2,†}, Ji-Soo Choi ^{3,4}, Hye Young Ji ³, Eunsuk Yang ¹, Joon Seok Park ³, Hyung Sik Kim ⁴, Min-Joo Kim ², In-Kyung Cho ², Suk-Jae Chung ^{1,5}, Yoon-Jee Chae ^{6,*} and Kyeong-Ryon Lee ^{2,7,*}

¹ College of Pharmacy, Seoul National University, Seoul 08826, Republic of Korea

² Laboratory Animal Resource Center, Korea Research Institute of Bioscience and Biotechnology, Cheongju 28116, Republic of Korea

³ Life Science Institute, Daewoong Pharmaceutical, Yongin 17028, Republic of Korea

⁴ School of Pharmacy, Sungkyunkwan University, Suwon 16419, Republic of Korea

⁵ Research Institute of Pharmaceutical Sciences, Seoul National University, Seoul 08826, Republic of Korea

⁶ College of Pharmacy, Woosuk University, Wanju-gun 55338, Republic of Korea

⁷ Department of Bioscience, University of Science and Technology, Daejeon 34113, Republic of Korea

* Correspondence: yjchae@woosuk.ac.kr (Y.-J.C.); kyeongrlee@kribb.re.kr (K.-R.L.)

† These authors contributed equally to this work.

Abstract: Enavogliflozin is a sodium-dependent glucose cotransporter 2 (SGLT2) inhibitor approved for clinical use in South Korea. As SGLT2 inhibitors are a treatment option for patients with diabetes, enavogliflozin is expected to be prescribed in various populations. Physiologically based pharmacokinetic (PBPK) modelling can rationally predict the concentration–time profiles under altered physiological conditions. In previous studies, one of the metabolites (M1) appeared to have a metabolic ratio between 0.20 and 0.25. In this study, PBPK models for enavogliflozin and M1 were developed using published clinical trial data. The PBPK model for enavogliflozin incorporated a non-linear urinary excretion in a mechanistically arranged kidney model and a non-linear formation of M1 in the liver. The PBPK model was evaluated, and the simulated pharmacokinetic characteristics were in a two-fold range from those of the observations. The pharmacokinetic parameters of enavogliflozin were predicted using the PBPK model under pathophysiological conditions. PBPK models for enavogliflozin and M1 were developed and validated, and they seemed useful for logical prediction.

Keywords: enavogliflozin; DWP16001; GCC5694A; sodium-glucose cotransporter 2 inhibitor; diabetes mellitus; physiologically based pharmacokinetic modelling; pharmacokinetics; mechanistic kidney model; in vitro–in vivo extrapolation



Citation: Kim, M.-S.; Song, Y.-K.; Choi, J.-S.; Ji, H.Y.; Yang, E.; Park, J.S.; Kim, H.S.; Kim, M.-J.; Cho, I.-K.; Chung, S.-J.; et al. Physiologically Based Pharmacokinetic Modelling to Predict Pharmacokinetics of Enavogliflozin, a Sodium-Dependent Glucose Transporter 2 Inhibitor, in Humans. *Pharmaceutics* **2023**, *15*, 942. <https://doi.org/10.3390/pharmaceutics15030942>

Academic Editor: Elżbieta Wyska

Received: 1 February 2023

Revised: 9 March 2023

Accepted: 12 March 2023

Published: 14 March 2023



Copyright: © 2023 by the authors. Licensee MDPI, Basel, Switzerland. This article is an open access article distributed under the terms and conditions of the Creative Commons Attribution (CC BY) license (<https://creativecommons.org/licenses/by/4.0/>).

1. Introduction

Glucose is a critical substrate of metabolism in eukaryotic organisms, and the homeostasis of blood glucose levels is essential for preventing metabolic disorders, including diabetes. Glucose is freely filtered through the renal glomerulus and enters the tubular system of the kidney. However, in healthy individuals, filtered glucose is almost completely reabsorbed in the proximal tubule. Therefore, glucose is absent or present at very low concentrations in the urine, and the loss of glucose is minimized.

Sodium-dependent glucose cotransporters (SGLTs) mediate glucose reabsorption against concentration gradients by coupling glucose transport and sodium transport. There are two well-known types of SGLTs in the kidney: SGLT1 and SGLT2 [1]. SGLT1 plays a minor role in renal glucose reabsorption [2]. Simultaneously, most of the glucose reabsorption in the kidney is mediated by the SGLT2, primarily localized in the S1 segment of the proximal tubule in the kidney [1–4]. Therefore, SGLT2 inhibitors have recently emerged as

one of the most promising glucose-lowering therapeutic agents. By selectively inhibiting the tubular reabsorption of glucose, SGLT2 inhibitors promote the urinary excretion of glucose and lower blood glucose levels [1].

Enavogliflozin (DWP16001) is a selective SGLT2 inhibitor developed by Daewoong Pharmaceutical Co., Ltd. (Seoul, Republic of Korea) and approved on 30 November 2022 by the Ministry of Food and Drug Safety for clinical use in South Korea (product name: Envlo Tablet) [1,5]. In Phase I clinical trials, enavogliflozin showed rapid absorption with a peak plasma concentration occurring 1–3 h post-administration and a long terminal half-life of 13–29 h in single and repeated oral administrations [6]. The systemic exposure of enavogliflozin increased dose proportionally after repeated administrations in the dose range of 0.1–2.0 mg [6]. However, the fraction of urinary-excreted enavogliflozin was increased along with increasing dose after a single administration in the dose range of 0.2–5.0 mg (i.e., from 0.87% to 1.67%) [6]. In this study, the PBPK model for enavogliflozin and M1 was developed based on the reported clinical trial data in the literature (ClinicalTrials.gov: NCT03364985), whose concentration-time profiles were collected after a single or repeated dosing of enavogliflozin [6].

Certain drug metabolites may be pharmacologically and/or toxicologically meaningful, and the United States Food and Drug Administration has suggested qualifying them when they are present more than 10 percent of total drug-related exposure [7]. Enavogliflozin appears to be metabolized in the human liver microsome system and generates metabolites, such as M1 (that is, (2S,3R,4R,5S,6R)-2-(7-chloro-6-(4-cyclopropylbenzyl)-2-hydroxy-2,3-dihydrobenzofuran-4-yl)-6-(hydroxymethyl)tetrahydro-2H-pyran-3,4,5-triol) and M2 (that is, (2S,3R,4R,5S,6R)-2-(7-chloro-6-(4-(1-hydroxycyclopropyl)benzyl)-2,3-dihydrobenzofuran-4-yl)-6-(hydroxymethyl)tetrahydro-2H-pyran-3,4,5-triol) [8]. In a previous clinical trial, the metabolic ratio of M1 was estimated between 0.20 and 0.25 after daily oral administration of 0.1 to 2.0 mg enavogliflozin in humans [6]. In this study, physiologically based pharmacokinetic (PBPK) models for enavogliflozin and M1 were developed and validated using the published concentration–time profiles of the compounds in humans.

Enavogliflozin is believed to be a treatment option for patients with diabetes who have a high chance of suffering from hepatic impairment and nephrotic syndrome [9]. PBPK models can rationally predict concentration–time profiles compared to conventional compartment models for first-in-human, special populations, drug–drug interactions, and pathophysiological situations [10–14]. As quantitative measures of physiological changes have been reported in the patients with hepatic impairment [12], the developed PBPK model could be used in pharmacokinetic predictions for the special populations in further studies.

The objective of this study was to develop and validate a PBPK model for orally administered enavogliflozin in humans.

2. Materials and Methods

2.1. Model Structure

To predict compound concentrations, PBPK models for enavogliflozin and metabolite M1 were developed. Whole-body PBPK models consisted of 15 and 13 compartments for enavogliflozin and M1, respectively, including the arterial/venous blood pool and the major tissues (Figure 1). For the kidney compartments, mechanistically arranged kidney sub-compartments were assumed based on the anatomical structure of the tissues, as described in the mechanistic kidney model section below. The anatomical weight and blood flow rates of the tissues were obtained from published data (Davies and Morris, 1993; Brown et al., 1997) [13,15,16] and are summarized in Table 1.

Numerical simulations of the PBPK models were performed using Berkeley Madonna software version 10.4.2 (Berkeley Madonna, Inc., Albany, CA, USA). In the present study, the fourth-order Runge–Kutta method was used for numerical integration. Because there were two PBPK models for the two compounds (enavogliflozin and M1), the compound for parameters were specified in a form of subscripts if it is needed.

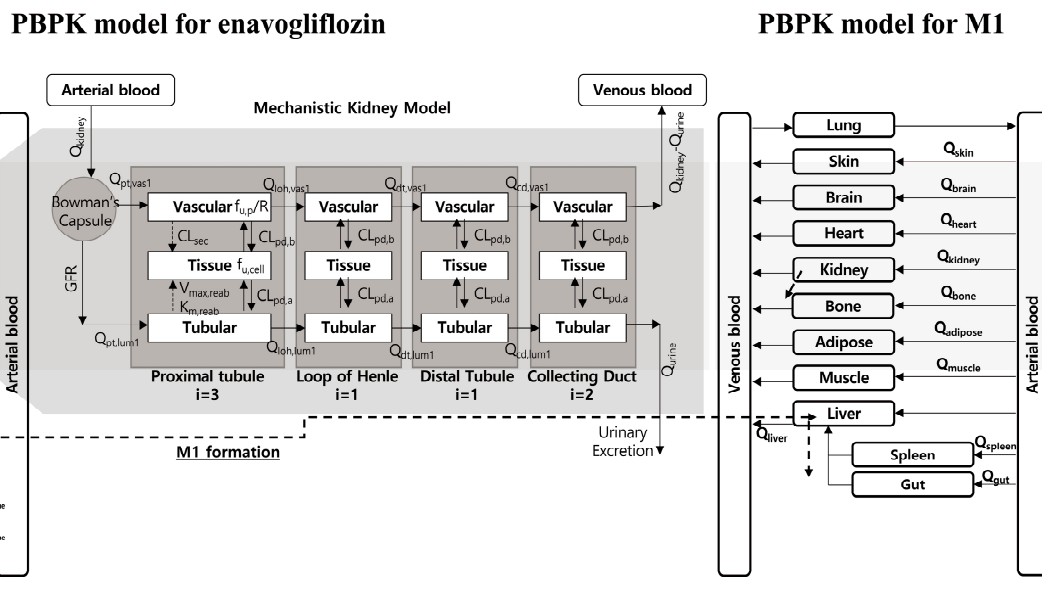


Figure 1. PBPK model scheme for enavoglitazone and metabolite M1 in humans after oral administration of enavoglitazone.

Table 1. Physiological parameters used for the whole body PBPK of enavoglitazone. The cardiac output for a representative human of 70 kg body weight was assumed to be 5200 mL/min.

Tissue	Anatomical Weight (g) ¹	Blood Flow (mL/min) ¹
Adipose	15,000	270
Bone	10,000	218
Brain	1400	593
Heart	329	208
Kidney	308	910
Large intestine	371	208
Liver	1800	1326
Lung	532	5200
Muscle	28,000	884
Skin	2600	260
Small intestine	637	520
Spleen	182	104
Stomach	147	52
Venous blood	3470	
Arterial blood	1730	

¹ The relative weight and flow were obtained from the literature [13,15,16].

2.2. Absorption

A first-order kinetics was used to describe the absorption of enavoglitazone in humans. The differential equation for the enteral compartment (i.e., the absorption compartment) is:

$$\frac{dX_a}{dt} = -K_a \cdot X_{a,enavo} \quad (1)$$

where $X_{a,enavo}$ is the amount of enavoglitazone remaining in the absorption compartment (e.g., the intestinal lumen), and K_a is the first-order absorption rate constant. The initial amount of enavoglitazone in the absorption compartment was set to be the product of F_a (i.e., fraction absorbed, predicted as 86.6%), F_g (i.e., not metabolized fraction in the gastrointestinal tract, assumed as 1), and the administered dose.

Drug permeability in the human jejunum was predicted by the empirical relationship between Caco-2 permeability (P_{app} ; 10^{-6} cm/s) in vitro and jejunum effective permeability (P_{eff} ; 10^{-4} cm/s) in vivo using the following empirical correlation [17]:

$$\log P_{eff} = 0.4926 \times \log P_{app} - 0.1454 \quad (2)$$

In this study, the experimentally determined Caco-2 P_{app} value of enavoglitazone (2.4×10^{-6} cm/s) was scaled using propranolol as a reference compound (i.e., P_{app} was multiplied by a scaling factor of 2.8) to fit the literature's values [17]. Subsequently, the fraction of the drug absorbed (F_a) was predicted using the relationship between the effective permeability (P_{eff}) using the following equation and the reported value in the literature [18]:

$$F_a = 1 - e^{-2 \cdot \frac{T_{res}}{r} \cdot P_{eff}} \quad (3)$$

where T_{res} is the transit time in the small intestine (~3 h) [18] and r is the radius of the small intestine. The first-order absorption rate (K_a) was also predicted by its relationship with the human jejunum effective permeability coefficient (i.e., $K_a = 2 \cdot P_{eff} / r$), in which the human intestinal tract is assumed to be a cylindrical tube.

2.3. Distribution

For enavoglitazone and M1, a perfusion-limited distribution was assumed for all tissue compartments, except the liver model of enavoglitazone. For tissues following perfusion-limited distribution, the differential equation for non-eliminating organs (i.e., tissues except for the liver and kidney) was as follows:

$$V_T \cdot \frac{dC_T}{dt} = Q_T \cdot \left(C_{art} - \frac{C_T \cdot R}{K_p} \right) \quad (4)$$

where V_T is the anatomical volume of the tissue compartment, C_T and C_{art} are the enavoglitazone or M1 concentrations in the tissue and arterial blood compartments, respectively, Q_T is the blood flow to the tissue, R is the blood-to-plasma partition coefficient, and K_p is the tissue-to-plasma partition coefficient. For the lung compartment, the input blood flow was from the venous blood pool, and C_{art} in the equation above was substituted by the compound concentration in the venous blood pool [i.e., $V_{LU} \cdot \frac{dC_{LU}}{dt} = Q_{LU} \cdot \left(C_{ven} - \frac{C_{LU} \cdot R}{K_{p,LU}} \right)$].

For the liver compartment, the enavoglitazone concentration in the input blood flow could be estimated using the following equation:

$$Q_{LI} \cdot C_{in,env} = K_a \cdot X_{a,env} + (Q_{LI} - Q_{ST} - Q_{SP} - Q_{Sm,IN} - Q_{La,IN}) \cdot C_{art,env} + Q_{ST} \cdot \frac{C_{ST,env} \cdot R_{env}}{K_{p,ST,env}} + Q_{SP} \cdot \frac{C_{SP,env} \cdot R_{env}}{K_{p,SP,env}} + Q_{Sm,IN} \cdot \frac{C_{Sm,IN,env} \cdot R_{env}}{K_{p,Sm,IN,env}} + Q_{La,IN} \cdot \frac{C_{La,IN,env} \cdot R_{env}}{K_{p,La,IN,env}} \quad (5)$$

where $C_{ST,env}$, $C_{SP,env}$, $C_{Sm,IN,env}$, and $C_{La,IN,env}$ are the enavoglitazone concentrations in the stomach, spleen, and small and large intestine, respectively; Q_{LI} , Q_{ST} , Q_{SP} , $Q_{Sm,IN}$, and $Q_{La,IN}$ are the blood flow to the liver, stomach, spleen, and small and large intestine, respectively; and $K_{p,LI,env}$, $K_{p,ST,env}$, $K_{p,SP,env}$, $K_{p,Sm,IN,env}$, and $K_{p,La,IN,env}$ are the tissue-to-plasma partition coefficients for the liver, stomach, spleen, and small and large intestine for enavoglitazone, respectively.

In the in vitro non-clinical study, enavoglitazone appeared to be a substrate for OATP1B1 and OATP1B3 transporters, and the respective K_m values were 39.6 and 50.6 $\mu\text{mol/L}$ in the transiently transporter-expressing HEK293 cells (Corning, Tewksbury, MA, USA). Permeability- and perfusion-limited models were integrated for the liver in the enavoglitazone model to describe the contribution of hepatic uptake transporters (e.g., OATP1B1 and OATP1B3). The integrated model, referred to as Model 1, is called the TUBE model by Jeong et al. [19,20] and is a generalized form of the extended clearance concept [21]. Passive diffusion was estimated

from the published correlation between physicochemical properties and passive permeability [22]. Even though, there was some clue for the active transport into the liver, specific value for the active permeability term was optimized based on the clinical trial data [6]. The observed concentration-time profiles after a single oral administration of 1 mg enavogliflozin to humans [6] using nonlinear regression method incorporated in the Curve Fit function of Berkeley Madonna software version 10.4.2 after assuming a linear kinetics in the uptake process. The effective surface area was allometrically scaled from the literature (Table S1) [20,23]. The distribution fraction for enavogliflozin to the liver ($f_{d,LI,enavo}$) was calculated as below:

$$f_{d,LI,enavo} = 1 - e^{\left[\frac{-PS_{inf,enavo} \cdot f_{up,enavo}}{Renavo \cdot Q_{LI}} \right]} \quad (6)$$

where $PS_{inf,enavo}$ is the uptake clearance from the extracellular compartment in the liver into hepatocytes for enavogliflozin. Consequently, the enavogliflozin in the liver compartment was calculated using the following equation:

$$V_{LI} \cdot \frac{dC_{LI,enavo}}{dt} = Q_{LI} \\ \cdot \left\{ C_{in,enavo} \cdot (1 - f_{d,LI,enavo}) + \frac{PS_{eff,enavo}}{PS_{inf,enavo}} \cdot \frac{f_{u,LI,enavo}}{f_{up,enavo}} \cdot Renavo \right. \\ \left. \cdot C_{LI,enavo} \cdot f_{d,LI,enavo} - CL_{u,int,enavo} \cdot f_{u,LI,enavo} \cdot C_{LI,enavo} \right\} \quad (7)$$

where V_{LI} is the anatomical volume of the liver and $CL_{u,int,enavo}$ is the intrinsic clearance of enavogliflozin in the liver compartment that was estimated from in vitro microsomal clearance using microsomal protein per gram of liver (e.g., 40 mg protein/g liver) and the liver weight [16,24]. $f_{u,LI,enavo}$ is the unbound fraction of enavogliflozin in the hepatocyte compartments estimated from the predicted liver-to-plasma partition coefficient using Rodgers and coworker's method considering binding terms [25,26], and $PS_{eff,enavo}$ is the distributional clearance from the liver cells to extracellular space in the liver for enavogliflozin that consists of passive permeability.

For M1, the compound concentration in the input blood pool was estimated as follows:

$$Q_{LI} \cdot C_{in,M1} = (Q_{LI} - Q_{Gut} - Q_{SP}) \cdot C_{art,M1} + Q_{Gut} \cdot \frac{C_{Gut,M1} \cdot R_{M1}}{K_{p,Gut,M1}} + Q_{SP} \cdot \frac{C_{SP,M1} \cdot R_{M1}}{K_{p,SP,M1}} + CL_{u,int,enavo} \cdot f_{u,LI,enavo} \cdot C_{LI,enavo} \\ \cdot f_{m,M1} \cdot \frac{MW_{M1}}{MW_{enavo}} \quad (8)$$

where $C_{in,M1}$, $C_{art,M1}$, $C_{Gut,M1}$, and $C_{SP,M1}$ are the M1 concentrations in the input blood, arterial blood pool, gut, and spleen compartment, respectively; $K_{p,Gut,M1}$ and $K_{p,SP,M1}$ are the tissue-to-plasma partition coefficients for M1 in the gut and spleen compartments, respectively; $f_{m,M1}$ is the fraction of metabolism which forms M1 from enavogliflozin as a result of the hepatic metabolism of enavogliflozin; and MW_{enavo} and MW_{M1} are the molar masses of enavogliflozin and M1, respectively. Molar masses were necessary as the calculation was performed in the gram-based unit (i.e., not in mol unit).

For the venous blood compartment, the following equation was used:

$$V_{ven} \cdot \frac{dC_{ven}}{dt} = Q_{AD} \cdot \frac{C_{AD} \cdot R}{K_{p,AD}} + Q_{BR} \cdot \frac{C_{BR} \cdot R}{K_{p,BR}} + Q_{HE} \cdot \frac{C_{HE} \cdot R}{K_{p,HE}} + Q_{KI,out} \cdot \frac{C_{KI} \cdot R}{K_{p,KI}} + Q_{LI} \cdot \frac{C_{LI} \cdot R}{K_{p,LI}} + Q_{SK} \cdot \frac{C_{SK} \cdot R}{K_{p,SK}} + Q_{BO} \\ \cdot \frac{C_{BO} \cdot R}{K_{p,BO}} + Q_{MU} \cdot \frac{C_{MU} \cdot R}{K_{p,MU}} + Q_{RE} \cdot C_{art} - Q_{CO} \cdot C_{ven} \quad (9)$$

where V_{ven} is the anatomical volume of venous blood; C_{AD} , C_{BR} , C_{HE} , C_{KI} , C_{LI} , C_{SK} , C_{BO} , C_{MU} , and C_{ven} are enavogliflozin or M1 concentrations in the adipose, brain, heart, kidney, liver, skin, bone, muscle, and venous blood compartments, respectively; Q_{AD} , Q_{BR} , Q_{HE} , Q_{KI} , Q_{LI} , Q_{SK} , Q_{BO} , Q_{MU} , and Q_{RE} are the blood flows to the adrenal gland, adipose, brain, heart, kidney, liver, skin, bone, muscle, and the residual blood flow, respectively;

Q_{CO} is the cardiac output; and $K_{p,AD}$, $K_{p,BR}$, $K_{p,HE}$, $K_{p,KI}$, $K_{p,LI}$, $K_{p,SK}$, $K_{p,BO}$, and $K_{p,MU}$ are the tissue-to-plasma partition coefficients of adipose, brain, heart, kidney, liver, skin, bone, and muscle, respectively, for enavoglitlozin or M1. In the case of the kidney, the outflow of blood from the kidney was adjusted by the filtrate loss via the mechanistic kidney model (i.e., $Q_{KI,out} = Q_{KI,in} - Q_{urine}$).

The tissue-to-plasma partition coefficients (K_p) of the tissue compartments were predicted for enavoglitlozin and M1 according to the method described by Rodgers and Rowland [25,26]. In this study, the K_p value of adipose tissue was predicted using the octanol-to-water partition coefficient for enavoglitlozin ($\log P_{o:w}$) instead of the olive oil-to-water partition coefficient ($\log P_{vo:w}$) [25,26], as it provided a better fit to the observed data. The steady-state tissue-to-plasma concentration ratios ($K_{p,ss}$) were predicted using the predicted K_p ratios and extraction ratios for the liver (that is, $K_{p,ss} = K_p \cdot \left(1 - \frac{ER}{f_d}\right)$, where ER is the extraction ratio, and f_d is the distributional fraction into the tissue [19]). Using the anatomical tissue volumes in Table 1 and the predicted $K_{p,ss}$ values, the calculation of V_{ss} was conducted using the following equation [27,28]:

$$V_{ss} = V_p + V_{rbc} \cdot EP + \sum V_{T,i} K_{p,ss,i} \quad (10)$$

where V_p and V_{rbc} are the volumes of plasma and blood cells, respectively, and EP is the blood cells-to-plasma partition coefficient. EP was calculated as follows [28]:

$$EP = 1 + (R - 1) / Hct \quad (11)$$

where Hct is the hematocrit (0.45) and R is the blood-to-plasma partition coefficient.

The unbound fraction of enavoglitlozin in the plasma ($f_{up,enavo}$) was determined from the results of an experiment on 1 mg/mL enavoglitlozin in human blood plasma using a Rapid Equilibrium Dialysis kit (Thermo Fisher Scientific, Waltham, MA, USA) after 4 h of incubation at 37 °C. The f_{up} for M1 ($f_{up,M1}$) was predicted by a published model (accessible at <https://drumap.nibiohn.go.jp/>; accessed on 3 January 2023), which was trained using a large dataset [29]. The blood-to-plasma partition coefficients (R) of enavoglitlozin and M1 were predicted using ADMET Predictor software version 10.4 (Simulation Plus, Inc., Lancaster, CA, USA).

Albumin was assumed to be the binding protein for enavoglitlozin and M1 [12] because compounds are slightly acidic. The assumption was needed for the prediction of unbound fraction and blood-to-plasma partition coefficient in the patients with impaired liver [30]. The tissue bindings were adjusted using altered albumin concentrations and hematocrit values in the pathological condition. Tissue-to-plasma partition coefficients were adjusted using the altered unbound fraction in plasma, assuming that the unbound fractions in the tissues were not affected by the disease condition.

2.4. Elimination

In this study, elimination in the PBPK model consisted of both hepatic and renal clearances. Hepatic metabolism was in vitro–in vivo extrapolated using the results of microsomal stability. The microsomal stability of enavoglitlozin was observed temporally in a 0.25 mg microsomal protein/mL suspension with NADPH either with or without UDPGA. The unbound fraction of enavoglitlozin and M1 in the microsomal suspension was predicted by ADMET Predictor software version 10.4.0.5 64-bit edition (Simulation Plus, Inc., Lancaster, CA, USA) for the 1 mg protein/mL condition and adjusted to the real experimental condition (0.25 mg protein/mL; i.e., $f_{u,undiluted} = \frac{\frac{1}{D}}{\left(\frac{1}{f_{u,diluted}} - 1\right) + \frac{1}{D}}$, where

D is the dilution factor in the system [31,32]). As only 3% of a dose of the unchanged form was excreted as bile in bile duct-cannulated rats after oral administration of ^{14}C -enavoglitlozin [8], the contribution of bile elimination was neglected in the PBPK model for enavoglitlozin.

The amount excreted through the renal route occupied 0.87–1.67% of the total dose of enavogliflozin after a single dose in a clinical trial [6]. Thus, the contribution of renal excretion to the total elimination of enavogliflozin appeared to be minor. However, the kidney is thought to be a target tissue for enavogliflozin, and the fraction of renal excretion (f_e) seems to increase with increasing doses [6]. To estimate the relative change in enavogliflozin concentration in the kidney, a mechanistically arranged kidney model was used. Non-linear reabsorption was incorporated into the kidney model based on the mechanistically arranged model [33–35].

M1 is a metabolite of enavogliflozin. In a previous study, enavogliflozin was not significantly eliminated in the intestinal microsomal suspension. Briefly, $95.7 \pm 15.3\%$ or $111.1 \pm 26.2\%$ of the initial enavogliflozin remained after incubating $2 \mu\text{M}$ enavogliflozin for 120 min at 37°C in human intestinal microsomal suspensions with or without UDPGA in the system, respectively ($n = 3$), and there was no statistical difference among the measured % remaining in 5, 15, 30, 45, 60, and 120 min after incubation of enavogliflozin started in the intestinal microsome suspension ($p > 0.05$, one-way ANOVA). As enavogliflozin seemed to be metabolized primarily in the liver, the site of M1 formation was assumed to be the liver. The proportion of M1 formation ($f_{m,M1}$) was estimated from the ratio between the elimination clearance of enavogliflozin in human liver microsomes and the formation clearance of M1 in human liver microsomes. The formation rate of M1 was obtained from human liver microsomes and recombinant enzymes in the literature [8]. The rate of M1 formation in recombinant enzymes was scaled by the P450 abundance (i.e., 142 pmol/mg protein for CYP3A4 and 14 pmol/mg protein for CYP2C19) and intersystem extrapolation factors (ISEF) for CYP3A4 and 2C19 from the literature [36]. The mean ISEFs for CYP3A4 and 2C19 were 0.154 and 0.248, respectively, based on the intrinsic clearance of the reference compounds in the literature (i.e., midazolam, testosterone and nifedipine for CYP3A4, and S-mephenytoin for CYP2C19) [36]. The calculated formation fractions of M1 were estimated from both the recombinant enzyme and the human liver microsome system and compared. The formation in the PBPK model incorporated the results from the two systems (i.e., microsomes, recombinant enzymes). The formation rate of M1 and M2 was calculated using the Michaelis–Menten equation ($CL_{u,HLM,(M1 \text{ or } M2)} = \frac{v_{max,HLM,(M1 \text{ or } M2)}}{K_{m,HLM,(M1 \text{ or } M2)} \cdot f_{u,mic,enavo} + f_{u,LI,enavo} \cdot C_{LI,enavo}}$), where $C_{LI,enavo}$ and $f_{u,LI,enavo}$ are the enavogliflozin concentration and unbound fraction in the liver, and $v_{max,HLM,(M1 \text{ or } M2)}$ and $K_{m,HLM,(M1 \text{ or } M2)}$ are the maximum rate and Michaelis–Menten constants for M1 or M2 formation in the human liver microsomes) and reported constants [8]. The fraction of M1 and M2 formation ($f_{m,M1}$ and $f_{m,M2}$) was predicted dynamically, as follows:

$$f_{m,(M1 \text{ or } M2)} = \frac{CL_{u,HLM,(M1 \text{ or } M2)}}{CL_{u,int,mic,enavo}} \quad (12)$$

where $CL_{u,int,mic,enavo}$ is the unbound intrinsic clearance of enavogliflozin elimination in the liver microsome. (e.g., $f_{m,M1} = \frac{\left(\frac{v_{max,HLM,M1}}{K_{m,HLM,M1} \cdot f_{u,mic,enavo} + f_{u,LI,enavo} \cdot C_{LI,enavo}} \right)}{CL_{u,int,mic,enavo}}$). Since the unbound fraction in the recombinant enzyme system was not reported for enavogliflozin, the absolute formation clearance could not be converted from the recombinant enzyme to the microsome system. The contribution of isozymes were estimated using the scaled results of recombinant enzyme assay for the prediction of altered formation rate in the pathophysiological condition (e.g., $f_{m,3A4} = f_{m,M1} \cdot \frac{\frac{v_{max,3A4,M1}}{K_{m,3A4,M1}}}{\frac{v_{max,3A4,M1}}{K_{m,3A4,M1}} + \frac{v_{max,2C19,M1}}{K_{m,2C19,M1}}} + f_{m,M2} \cdot \frac{\frac{v_{max,3A4,M2}}{K_{m,3A4,M2}}}{\frac{v_{max,3A4,M2}}{K_{m,3A4,M2}} + \frac{v_{max,2C19,M2}}{K_{m,2C19,M2}}}$).

Altered elimination of enavogliflozin was predicted based on the reported model parameters with liver cirrhosis in the literature [12]. The changed activity of CYP2C19 enzyme is calculated from the reported plasma clearance of mephenytoin and formation of 4-hydroxymephenytoin [37], and functional liver mass [12] in the patients with liver cirrhosis. There were no accessible observations about M1 elimination. Metabolic rate and renal clearance for M1 were predicted using the published methods (accessible at [https:](https://)

//drumap.nibiohn.go.jp/; accessed on 3 January 2023) [38,39]. The predicted microsomal intrinsic clearance for M1 was assumed to be unbound one, as the literature handled the intrinsic clearance with unbound concentration (that is, Equation (2) of the literature: $CL_h = Q_h \cdot \frac{f_{up} \cdot CL_{u,int}}{Q_h + f_{up} \cdot CL_{u,int}}$) [38].

2.5. Mechanistic Kidney Model

A mechanistic kidney model for enavogliflozin was developed to predict its non-linear urinary excretion mainly based on the model structures and values with slight changes reported by Pletz et al. [33] and Scotcher et al. [34,35]. Because the mechanistic kidney model in this study was utilized only for the enavogliflozin (Figure 1), the compound name was not specified on the name of model parameters for the kidney model. The mechanistic kidney model consists of 21 compartments, reflecting the physiological segmentations of the kidney [33–35]. The kidney is divided into four major segments (i.e., proximal tubule, loop of Henle, distal tubule, and collecting duct), which are further divided into subsegments (i.e., three subsegments for proximal tubule, one subsegment for the loop of Henle and distal tubule each, and two subsegments for the collecting duct). Each subsegment is divided into three compartments: tubular lumen, cellular compartment, and vascular blood section (Figure 1). The volumes and tubular flow rates of each segment of the kidney were obtained from the literature [33–35] and are listed in Tables S2 and S3. The unbound fraction in the kidney cells for enavogliflozin ($f_{u,cell}$) was estimated from the predicted tissue-to-plasma partition coefficient using Rodgers and coworker's method [25,26,30], which incorporated various binding terms. In the kidney model, the Michaelis–Menten kinetics model was assumed for non-linear reabsorption, which describes the observed non-linearity in the fraction of renal excretion (f_e). The constants for the Michaelis–Menten equation (i.e., $K_{m,reab}$ and $v_{max,reab}$) and a secretory clearance (CL_{sec}) were optimized using the observed enavogliflozin amount in urine after a single oral administration of 0.2–5 mg enavogliflozin in humans (training set), and validated using the enavogliflozin concentration in urine after repeated administration of enavogliflozin in humans (validation set). A detailed description of the kidney sub-compartments is provided in Appendix A along with the mass-balanced equations (Equations (A1)–(A14)).

2.6. Modelling Strategies

The results from the clinical trials were obtained from Daewoong Pharmaceutical Company and have already been published in an academic journal (ClinicalTrials.gov: NCT03364985) [6]. The observed concentration-time profiles were divided into two groups, the training and validation sets. During the model refinement process, results from a single-dose oral administration study of enavogliflozin ranging from 0.2 to 5 mg were used. For model validation, a repeated administration study for 15 days with doses ranging from 0.3 to 1 mg/day was used. There was no training set for the M1 model, and the M1 concentration-time profiles after repeated administration were utilized for model validation.

The proposed PBPK model was validated by comparing the AUC_{inf} , AUC_τ (i.e., area under the plasma concentration–time curve from time zero to infinity at the single dosing regimen and a dosing period at the repeated dosing regimen, respectively), and C_{max} (i.e., the maximum plasma concentration) values from the simulations to those from the clinical data of repeated administration studies. In the present study, the fold differences of the resulting AUC ratios ($AUC_{pred}:AUC_{obs}$) and C_{max} ratios ($C_{max,pred}:C_{max,obs}$) within a factor of two (0.5–2) were considered adequate for model performance estimation [13]. In the case of enavogliflozin in urine, model performance was assessed based on the ratio between the simulated and observed excreted amounts at the last sampling time after a single administration. The mean amounts and concentrations were used as the observed values for the model validation.

2.7. Statistics and Data Analysis

Statistical differences between two groups were determined using Student's *t*-test, and one-way ANOVA was used for multiple comparisons. In the present study, data were expressed as means \pm standard deviation (S.D.), and *p*-values < 0.05 denoted statistical significance.

Standard non-compartmental analysis was performed using WinNonlin software version 8.1 (Pharsight Corporation, Mountain View, CA, USA) and the web-based Blueberry service (accessible at <https://pk-square.com>; accessed on 3 January 2023). Microsoft Excel software version 2211 (Microsoft Corporation, Redmond, WA, USA) was used for the unpaired *t*-tests and visualization of the simulation. GraphPad Prism software version 9.5.0 (GraphPad Software, San Diego, CA, USA) was used to visualize the simulations. Web-based Chemicalize service (ChemAxon Kft., Budapest, Hungary; accessible at <https://chemicalize.com/>; accessed on 3 January 2023) was used to obtain several physicochemical properties.

3. Results

3.1. Optimization of the PBPK Model

The input parameters for the PBPK model were derived from in silico and in vitro studies and are summarized in Table 2. The kinetic parameters involved in absorption were derived from the Caco-2 permeability of enavogliflozin. Enavogliflozin was predicted to be rapidly absorbed (K_a value of 0.764 h^{-1}) with good permeability through intestinal membranes (F_a value of 0.866). The unbound fraction in plasma (f_{up}) was observed as 0.015 ± 0.002 for enavogliflozin and predicted as 0.080 for the metabolite M1 [29]. The extent of distribution was derived from the in silico prediction of tissue partition coefficients (K_p). The volumes of distribution at steady state (V_{ss}) were predicted to be 1.44 L/kg for enavogliflozin and 0.431 L/kg for the metabolite M1.

Preclinical data suggest that enavogliflozin is primarily eliminated by hepatic pathways, including metabolism and bile excretion. Indeed, phase I clinical data reports that renal excretion of enavogliflozin is negligible (less than 2.5%) in humans [6]. Therefore, the predicted metabolic clearance was assumed to be the only intrinsic clearance in the liver. The unbound fraction of enavogliflozin in microsomal suspension was predicted to be 0.577 in 1 mg protein/mL using ADMET Predictor software version 10.4.0.5 and adjusted to 0.845 in the 0.25 mg protein/mL condition after considering the dilution factor. The intrinsic clearance was obtained from an in vitro human microsomal stability assay ($13.5 \mu\text{L}/\text{min}/\text{mg protein}$), and the unbound clearance was calculated as $16.0 \mu\text{L}/\text{min}/\text{mg protein}$ for enavogliflozin. The unbound intrinsic clearance was incorporated into the model with physiological scalars (e.g., milligram protein per gram of the liver and liver weight in humans) [16,24]. There was no statistically significant difference in the intrinsic clearance of enavogliflozin with or without UDPGA in the human microsomal suspension based on the *t*-test (*p* = 0.329). The active uptake clearance ($PS_{u,inf,act,enavo}$) was optimized as 9.73 L/h/kg using the observed concentration–time profiles after a single oral administration of 0.2 to 5 mg enavogliflozin orally in humans (training set; Figure 2).

Table 2. Input parameters for PBPK modelling of enavogliflozin in humans.

Compound	Parameter	Unit	Value	Reference	
Enavogliflozin	Physicochemical properties	Molar mass	446.92	Chemicalize	
		Compound type	Neutral	Chemicalize	
		pKa (acidic)	12.57	Chemicalize	
		logP	2.65	[40]	
		f_{up}	0.015	Measured (See text)	
	Absorption	B/P ratio (R_{enavo})	0.720	Predicted (See text)	
		$P_{app,PAMPA}$	1.74	Predicted (See text)	
M1	Absorption	P_{eff}	10 ⁻⁴ cm/s	Predicted (See text)	
		K_a	h ⁻¹	Predicted (See text)	
		F_a	0.866	Predicted (See text)	
	Distribution	V_{ss}	L/kg	1.44	Predicted [25,26]
	Elimination	$CL_{int,enavo}$	μL/min/mg protein	13.5	Measured (See text)
		$f_{u,mic,enavo}$		0.845	Predicted (See text)
	Physicochemical properties	Molar mass	462.92	Chemicalize	
M2	Formation	Compound type	Neutral	Chemicalize	
		pKa (acidic)	11.92	Chemicalize	
		log P	1.982	Chemicalize	
		$f_{up,M1}$	0.080	Predicted [29]	
		B/P ratio (R_{M1})	0.724	Predicted (See text)	
	Distribution	$K_{m,HLM,M1}$	nmol/mL ¹	150.1	[8]
		$v_{max,HLM,M1}$	pmol/min/mg protein ¹	980.3	[8]
Formation		$K_{m,3A4,M1}$	nmol/mL ¹	471.4	[8]
		$v_{max,3A4,M1}$	pmol/min/mg protein ²	631.5	Estimated (See text)
		$K_{m,2C19,M1}$	nmol/mL ¹	156.4	[8]
		$v_{max,2C19,M1}$	pmol/min/mg protein ²	12.48	Estimated (See text)
	Distribution	V_{ss}	L/kg	0.421	Predicted [25,26]
	Elimination	$CL_{u,int,M1}$	μL/min/mg protein	30.542	Predicted [38]
		$CL_{r,M1}$	L/h/kg	0.04227	Predicted [39]
Formation		$K_{m,HLM,M2}$	nmol/mL ¹	58.7	[8]
		$v_{max,HLM,M2}$	pmol/min/mg protein ¹	82.8	[8]
		$K_{m,3A4,M2}$	nmol/mL ¹	674.5	[8]
		$v_{max,3A4,M2}$	pmol/min/mg protein ²	83.04	Estimated (See text)
		$K_{m,2C19,M2}$	nmol/mL ¹	35.4	[8]
		$v_{max,2C19,M2}$	pmol/min/mg protein ²	2.385	Estimated (See text)

¹ Total concentration of enavogliflozin in the microsomal suspension (i.e., the unbound fraction in the microsomal suspension was needed to estimate the unbound concentration). ² The maximum rate was adjusted to the milligram microsomal protein-based value after rationally scaled from the value in the assay using recombinant enzymes.

Renal excretion was predicted using a mechanistic kidney model that incorporated a non-linear reabsorption term for enavogliflozin in humans. The model parameters for the kidney were obtained after non-linear regression using the observed cumulative renal excretion after a single administration of enavogliflozin in humans. The obtained parameters were 0.0845 ng/mL, 305 ng/h and 3.39 L/h for $K_{m,reab}$, $v_{max,reab}$, and the secretory clearance (CL_{sec}), respectively.

Among the metabolites of enavogliflozin, the fractions for M1 and M2 formation ($f_{m,(M1 \text{ or } M2)}$) were estimated as 48.4% and 10.4% after comparing the intrinsic elimination clearance (13.5 μL/min/mg protein) for enavogliflozin and the formation clearance for M1 and M2 (6.53 μL/min/mg protein for M1 and 1.41 μL/min/mg protein for M2) in human microsomal suspension from the literature [8]. The f_m for M1 and M2 was also calculated based on the results of M1 and M2 formation rate in the recombinant enzymes. As the ISEF-CL_{int} and P450 abundance could be obtained from the literature [8,36], the results between the different isozymes (i.e., CYP3A4 and CYP2C19) were compared. The contribution of CYP3A4 for M1 and M2 formation were 94.4% and 64.6%, respectively, which was comparable to the results using specific antibodies in the literature [8]. Those of CYP2C19 for M1 and M2 were 5.62% and 35.3%, respectively. Thus, CYP3A4 and CYP2C19 appeared to cover 52.4% and 6.42% of enavogliflozin metabolism in the liver.

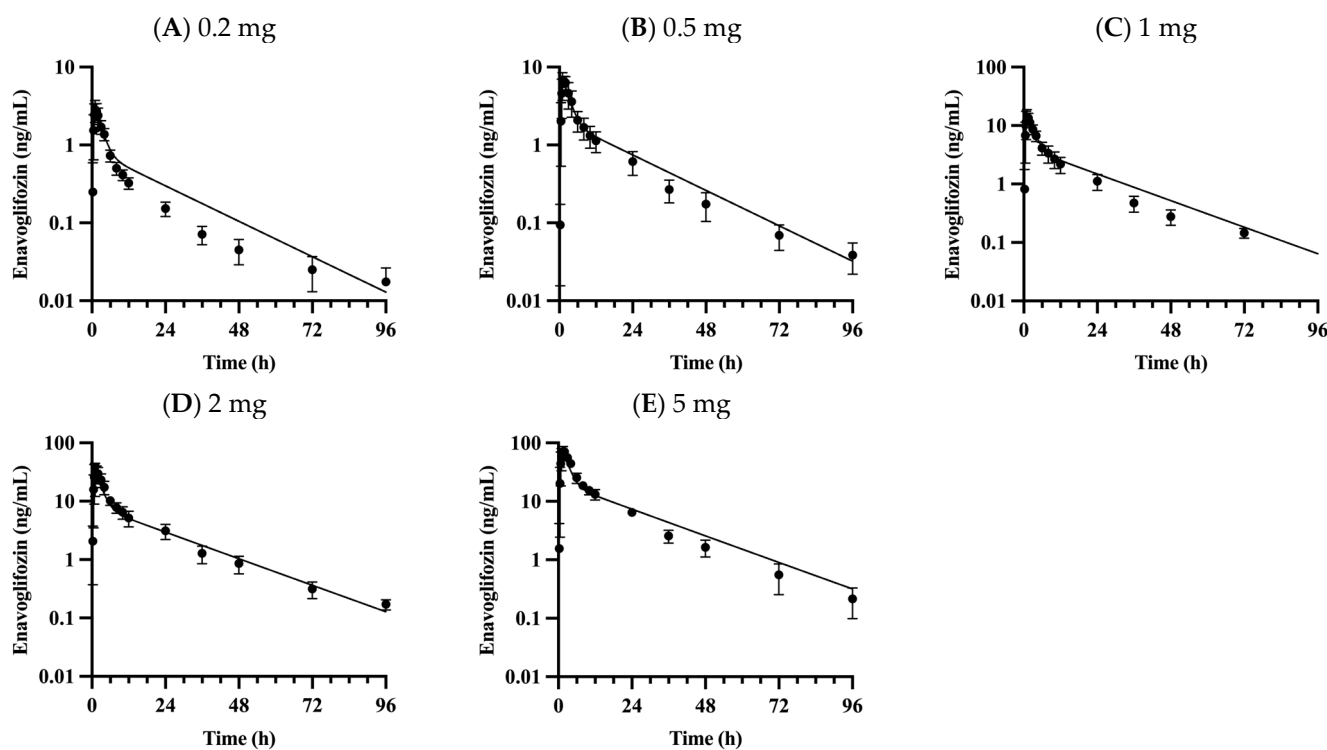


Figure 2. Observed and simulated plasma concentration profiles for enavoglitazin in humans following single doses of 0.2 (A), 0.5 (B), 1 (C), 2 (D), and 5 mg (E). Solid lines represent the optimized simulations, and closed circles (●) represent observed data. Data are expressed as means \pm S.D. from eight to ten healthy volunteers.

For the PBPK model of M1, the compound's elimination rate should be assigned. However, there were no accessible in vitro and in vivo experimental results for the metabolite M1. The unbound intrinsic clearance for M1 was predicted in silico to be $30.542 \mu\text{L}/\text{min}/\text{mg}$ protein [38]. The renal clearance was predicted in silico to be $42.27 \text{ mL}/\text{h}/\text{kg}$ by the published method [39].

3.2. Validation of the PBPK Model

The proposed PBPK model captured the plasma concentration–time profiles of enavoglitazin (Figure 2) following a single dose (0.2–5 mg enavoglitazin) and repeated doses (i.e., the validation set of 0.3, 0.5, 1 mg/day for 15 days; Figure 3) in humans. The estimated AUC_{inf} and C_{max} ratios between simulated and observed values ranged from 0.901 to 1.25 and from 0.812 to 1.04, respectively, after the single administration of enavoglitazin (Table 3). When the proposed model was used to predict the systemic pharmacokinetics of enavoglitazin obtained from the validation dataset (Figure 3), the AUC_{τ} and C_{max} ratios for the first day of administration ranged from 0.811 to 1.05 and 0.712 to 0.869, respectively. In addition, the AUC_{τ} and C_{max} ratios for the last day of administration ranged from 0.758 to 0.880 and 0.660 to 0.727, respectively (Table 3). Furthermore, the concentration–time profiles of M1 were predicted using the developed PBPK model (Figure 4). Because there were no optimized parameters in the M1 model, there was no training set for the M1 model among the clinical data. The AUC_{τ} ratio and C_{max} ratio of M1 were predicted and compared to those of the observed parameters after repeated enavoglitazin dosing in humans (Table 4). The AUC_{τ} ratio ranged from 0.762 to 1.06, and the C_{max} ratio was between 0.641 and 0.829 for M1 in the range of repeated enavoglitazin doses. The AUC ratio and C_{max} ratio were within the two-fold error range, which was assumed to be the acceptable range of the model performance in the method section. Collectively, the PBPK models developed in this study were found to be valid according to preset criteria.

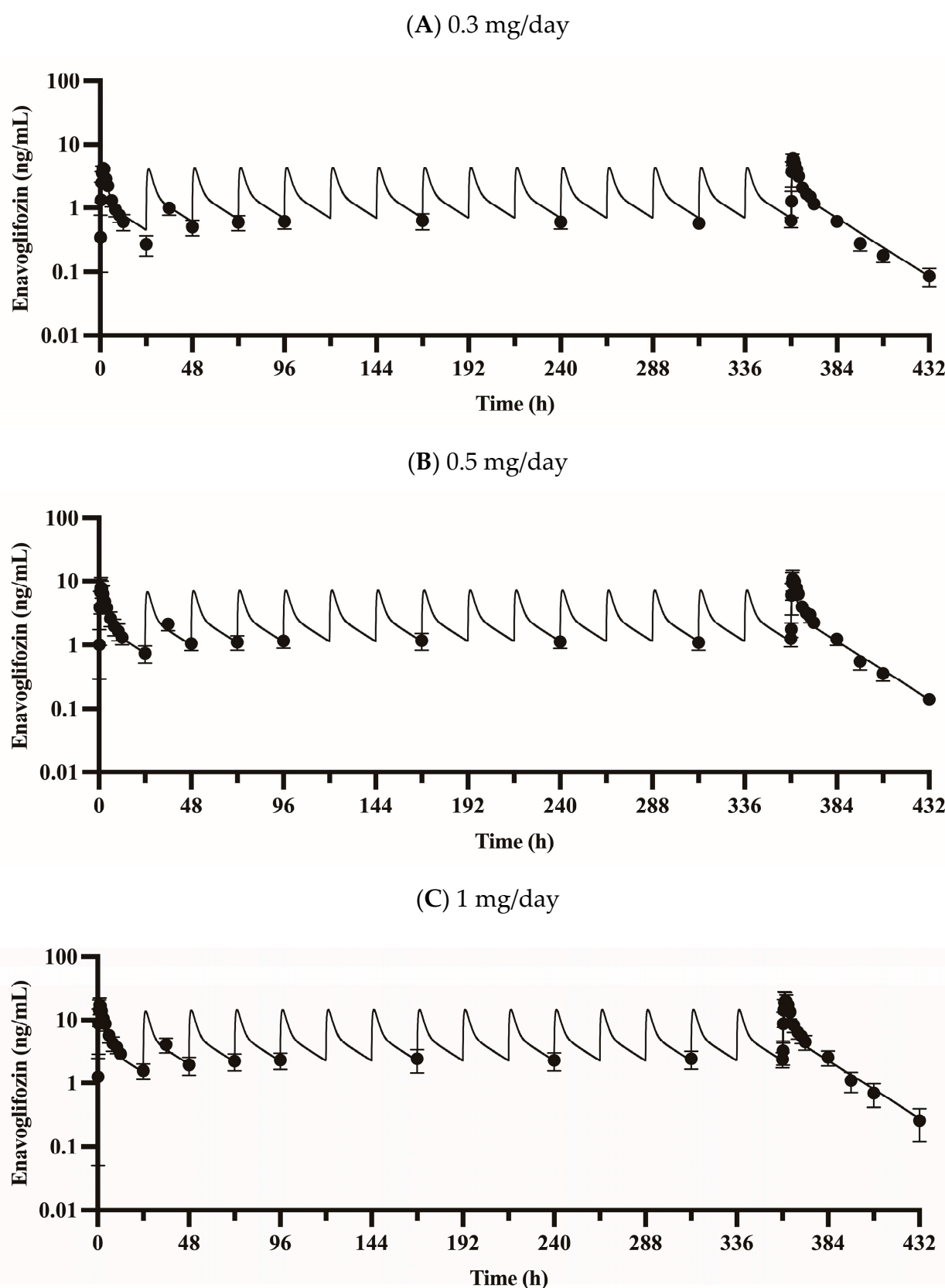


Figure 3. Observed and predicted plasma enavogliiflozin concentration profiles in humans during repeated doses of 0.3 (A), 0.5 (B), and 1 mg enavogliiflozin (C) administered once daily for 15 days. Solid lines represent the model prediction (i.e., simulated data), and closed circles (●) represent observed data. Data are expressed as means \pm S.D. from eight healthy volunteers.

A mechanism-based kidney model for enavogliflozin was developed using the urinary excretion profile of the drug administered within the dose ranges of 0.2–5 mg. The cumulative observed amounts of enavogliflozin in urine were 1.71 ± 0.463 , 5.85 ± 1.65 , 12.7 ± 2.34 , 32.0 ± 6.07 , and 81.6 ± 27.9 μg at the last sampling time for excretion after the single administration of 0.2, 0.5, 1, 2, and 5 mg of enavogliflozin in humans, respectively (training set) [6]. The simulated cumulative amounts of enavogliflozin excreted in urine were 1.93, 5.69, 12.8, 29.8, and 85.2 μg after the single administration of 0.2, 0.5, 1, 2, and 5 mg of enavogliflozin, respectively, at the same time point (Figure 5) [33–35]. The simulated amount of urinary-excreted enavogliflozin was in the two-fold range of the observed value at the last sampling time after any single dosage examined in humans.

Table 3. Summary of predicted and observed AUC (ng·h/mL) and C_{\max} (ng/mL) ratios of enavogliflozin in single dose and repeated dose administration studies.

Dose	$AUC_{\text{obs}}^{1,2}$ (ng·h/mL)	AUC_{pred}^1 (ng·h/mL)	AUC Ratio	$C_{\max,\text{obs}}$ (ng/mL)	$C_{\max,\text{pred}}$ (ng/mL)	C_{\max} Ratio
<i>Training set (the single dosing study)</i>						
0.2 mg	20.2	25.1	1.25	2.84	2.44	0.859
0.5 mg	53.2	62.6	1.18	5.87	6.11	1.04
1 mg	110	125	1.14	14.0	12.2	0.871
2 mg	277	249	0.901	30.1	24.4	0.812
5 mg	619	621	1.00	70.7	61.0	0.863
<i>Validation set (1st day of the repeated dosing study)</i>						
0.3 mg/day	26.2	27.4	1.05	4.22	3.67	0.869
0.5 mg/day	51.5	45.6	0.886	7.86	6.11	0.778
1 mg/day	112	91.0	0.811	17.2	12.2	0.712
<i>Validation set (15th day of the repeated dosing study)</i>						
0.3 mg/day	42.7	37.6	0.880	6.04	4.32	0.714
0.5 mg/day	82.4	62.5	0.758	10.9	7.19	0.660
1 mg/day	163	125	0.762	19.7	14.4	0.727

¹ AUC_{inf} and AUC_{τ} were calculated for the single and repeated dosing study, respectively. ² AUC_{obs} was calculated using the mean concentration–time profiles for each group.

Table 4. Summary of predicted and observed AUC_{τ} (ng·h/mL) and C_{\max} (ng/mL) ratios of M1 in the repeated dose administration studies.

Enavogliflozin Dose	AUC_{obs}^* (ng·h/mL)	AUC_{pred} (ng·h/mL)	AUC Ratio	$C_{\max,\text{obs}}$ (ng/mL)	$C_{\max,\text{pred}}$ (ng/mL)	C_{\max} Ratio
<i>Validation set (1st day of the repeated dosing study)</i>						
0.3 mg/day	5.73	6.05	1.06	0.725	0.564	0.779
0.5 mg/day	9.55	10.1	1.05	1.13	0.940	0.829
1 mg/day	22.3	20.1	0.901	2.56	1.88	0.734
<i>Validation set (15th day of the repeated dosing study)</i>						
0.3 mg/day	10.8	8.30	0.766	1.09	0.699	0.641
0.5 mg/day	17.0	13.8	0.811	1.80	1.16	0.646
1 mg/day	36.2	27.6	0.762	3.56	2.33	0.654

* AUC_{obs} was calculated using the mean concentration–time profiles for each group.

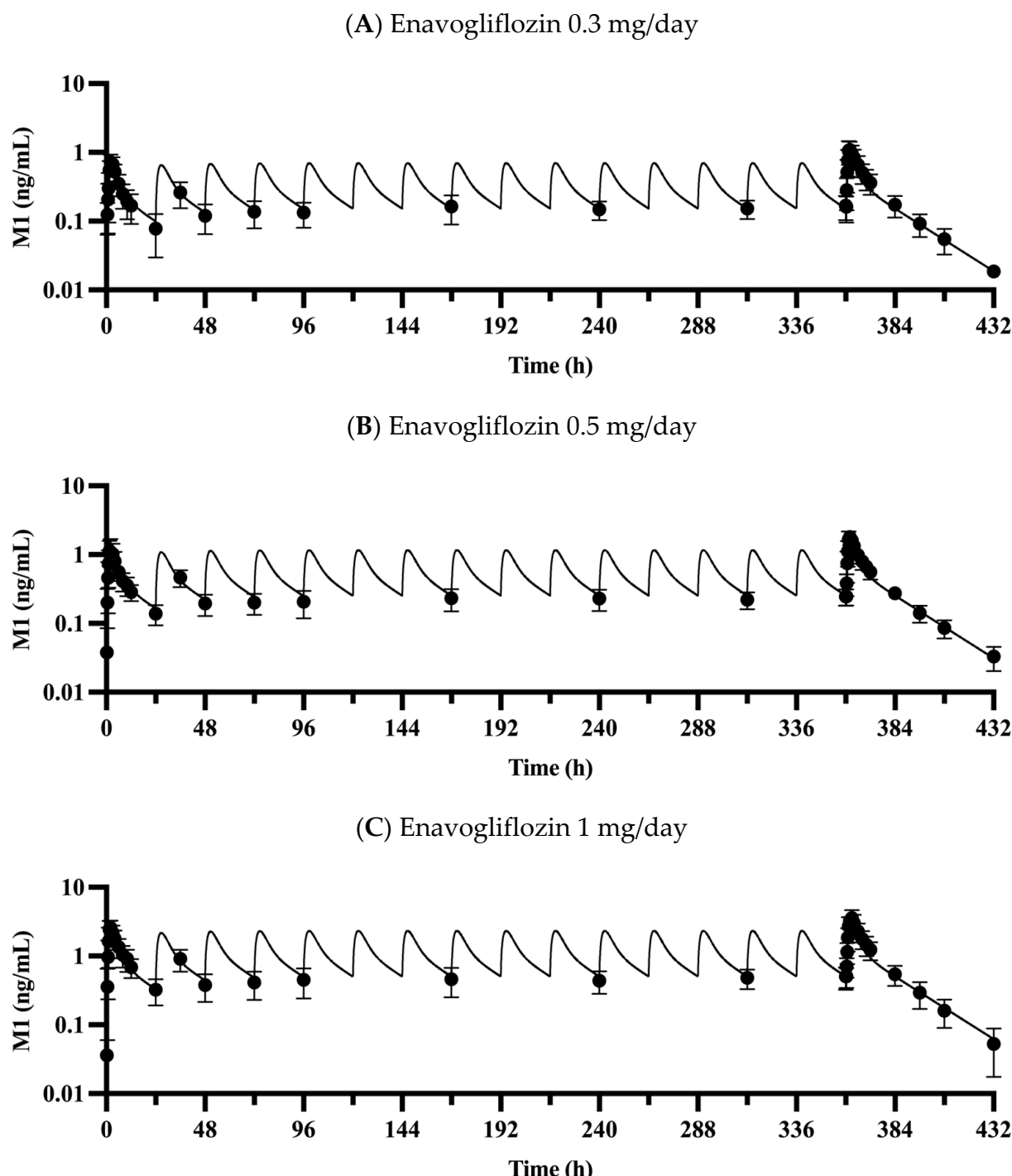


Figure 4. Observed and predicted plasma concentration profiles for the metabolite M1 at repeated doses of 0.3 (A), 0.5 (B), and 1 mg enavogliflozin (C) administered to humans once daily for 15 days. Solid lines represent the model predicted M1 concentration (i.e., simulated data), and closed circles (●) represent observed data. Data are expressed as means \pm S.D. from eight healthy volunteers.

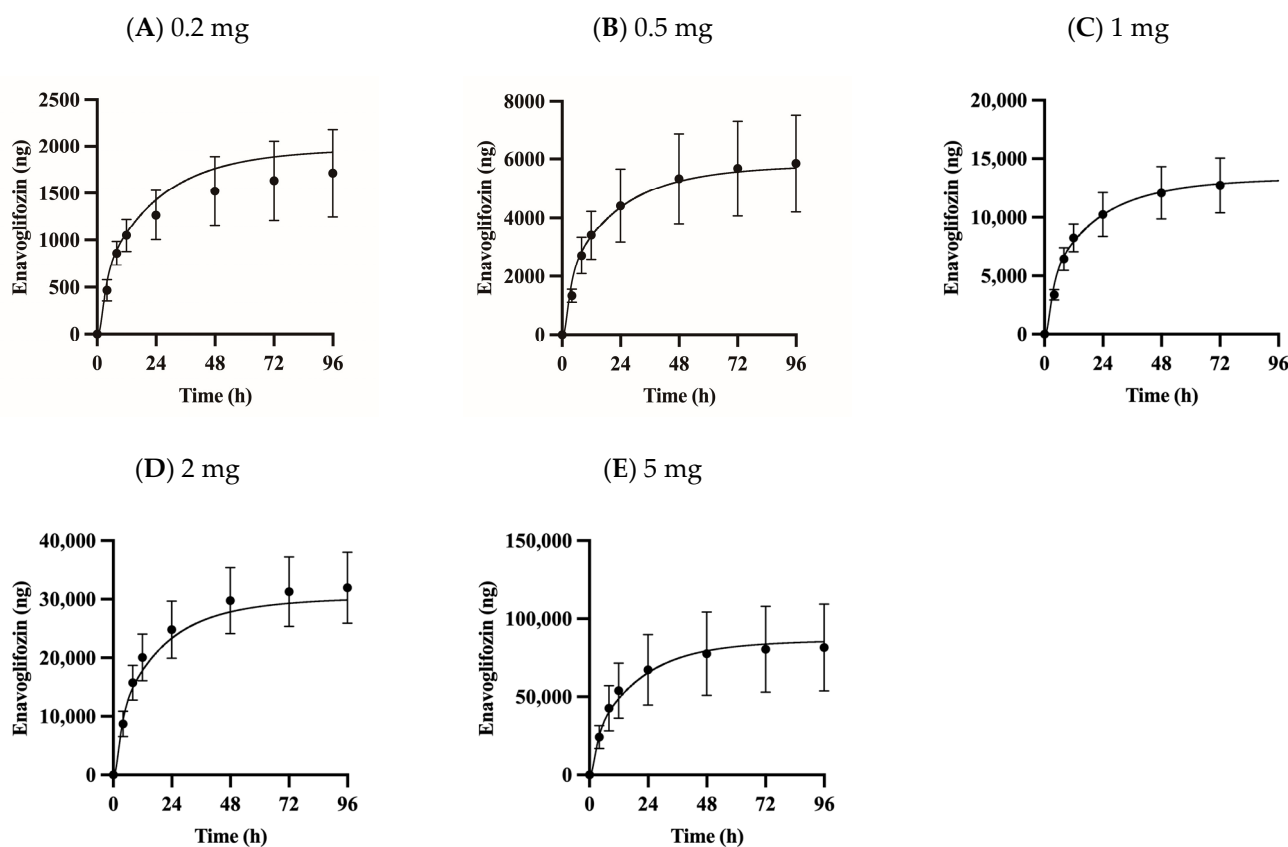


Figure 5. Cumulative urinary excretion profiles of enavogliflozin at single doses of 0.2 (A), 0.5 (B), 1 (C), 2 (D), and 5 mg (E) to humans. Solid lines represent the optimized simulations, and closed circles (●) represent observed data. Data are expressed as means \pm S.D. from eight healthy volunteers.

4. Discussion

This was the first study for publication to simulate concentration–time profiles of enavogliflozin and its metabolite M1 based on PBPK models in humans. In this study, PBPK models for enavogliflozin and its metabolite M1 were developed and validated using in silico and in vitro data accompanied by clinical observations. The PBPK model developed in this study can be used to extend dosing regimens and predict drug–drug interactions and population-related alterations in the pharmacokinetic profiles of enavogliflozin in humans. For example, some marketed drugs require their dosing regimen to be adjusted or are not recommended for patients with hepatic or renal impairment [12,41–43]. Additionally, researchers involved in new drug development may need to predict the expected exposure or concentration profiles of the agent before clinical observation. The model-based prediction would have a role in that decision, especially the PBPK model, because of the physiological factors it accounts for, even though the prediction might be verified after clinical trials in the patient population.

In a previous study, M1 was reported to have metabolic ratios (i.e., AUC ratio between M1 and enavogliflozin) of 25%, 21%, and 22% for the repeated doses of 0.3, 0.5, and 1 mg/day, respectively [6]. Based on the AUC_{τ} after the last dose of repeated administration study, the predicted metabolic rates for M1 were 18.8%, 16.2%, and 16.3% for the 0.3, 0.5, and 1 mg/day doses, respectively. The model appeared to reproduce the slight difference in metabolic rates seen among those doses. For the calculation of the metabolic rate, the AUC values of enavogliflozin and M1 were converted to molar-based values (i.e., not a gram-based unit, but a mol-based unit was incorporated). Though there were Michaelis–Menten constants for those two isozymes, CYP3A4 and CYP2C19, the same contribution ratio among the dose range was assumed because of the absence of the

unbound fraction in the recombinant enzyme system. The assumption may be reasonable because of the high Michaelis–Menten constant for those two isozymes (Table 2). Although the metabolic fraction for the formation of M1 ($f_{m,M1}$) was estimated from the in vitro assay, the volume of distribution (i.e., estimated by predicted K_p) and elimination rate for M1 [i.e., metabolism ($CL_{u,int,M1}$) and renal excretion ($CL_{r,M1}$)] were predicted using in silico methods [25,26,30,38,39]. Thus, the metabolic rate could be better predicted with more robust information on the formation, distribution, metabolism, and excretion of M1 (e.g., unbound fraction of enavogliflozin in the recombinant enzyme system, cumulatively excreted amount of M1 in vivo, and microsomal stability of M1 in vitro). In a published structure–activity relationship (SAR) study, hetero-bicyclic derivatives of enavogliflozin seemed to have similar IC₅₀ values for SGLT2 and showed a difference in their selectivity between SGLT1 and SGLT2 [1]. However, there were no experimental IC₅₀ values for the metabolite M1 in the SAR study. Further experiments and trials may be required to refine and extend the developed PBPK model along with pharmacodynamic model.

The simulated concentrations or amounts of enavogliflozin in plasma and urine, respectively, seemed to match well with observed profile (Figures 2–5), and the predicted pharmacokinetic parameters met the criteria (Tables 3 and 4). Therefore, the developed PBPK model was validated using the established criteria in this study. As a model challenge, the absolute bioavailability was predicted for oral administration in humans. This predicted bioavailability ranged from 78.9% to 79.0% after a single dose of 0.2, 0.5, 1, 2 and 5 mg and at the steady-state after repeated doses of once-daily administration of 0.3, 0.5 and 1 mg enavogliflozin. Although there have been no clinical trials testing intravenous doses, the predicted oral bioavailability in humans is comparable to the reported values in the animal experiments, which were 84.5–97.2% in mice and 56.3–77.4% in rats [1,44]. Even though the absorption model had a simple structure (i.e., the first-order kinetics), the predicted exposure (AUC) and C_{max} matched to the observed values well. However, a more sophisticated model for the absorption (e.g., CAT, A-CAT, and ADAM models) might be needed to study the absorption level alteration [45–48].

In the aspects of intestinal metabolism, there were experimental results for enavogliflozin using human intestinal microsome that showed no statistically meaningful elimination ($p > 0.05$, one-way ANOVA test for each measuring time) in the intestinal microsomal suspension with NADPH only or with both NADPH and UDPGA. Briefly, the percent remaining after incubation were $97.2 \pm 24.2\%$, $109.8 \pm 26.2\%$, $117.5 \pm 27.8\%$, $96.4 \pm 7.2\%$, $101.2 \pm 22.9\%$, and $111.1 \pm 26.2\%$ for 5, 15, 30, 45, 60, and 120 min, respectively, after the initiation of incubation with NADPH only, and $106.7 \pm 3.8\%$, $110.2 \pm 5.7\%$, $107.5 \pm 10.2\%$, $87.2 \pm 10.9\%$, $90.5 \pm 10.1\%$, and $95.7 \pm 15.3\%$ for 5, 15, 30, 45, 60, and 120 min, respectively, after the incubation starts with NADPH and UDPGA. Though there was no statistical significance among the measured percent remaining, the variability of the measure was larger than the results in the liver microsomal suspension, especially in the group with NADPH only. Because CYP enzymes had a meaningful contribution to the liver metabolism, there might be unseen contributions of the drug-metabolizing enzymes in the intestine.

The elimination in the kidney can be attributed to excretion and metabolism [49]. In this study, renal elimination in the PBPK model of enavogliflozin was achieved via urinary excretion. Enavogliflozin revealed a dose-dependent increase in the fraction excreted in urine, and the kidney model for enavogliflozin incorporated nonlinearity in the reabsorption term. Additional observations for renal elimination can be incorporated into the kidney model for future studies, such as predicting the pharmacological effect of enavogliflozin based on pharmacodynamic modelling in humans. Despite this limitation, the PBPK model could simulate the cumulative amounts of urinary excretion of enavogliflozin in the pre-set range of error (i.e., 2-fold) after a single administration of the drug orally in humans (Figure 5).

Based on the model simulation (Figure 6), the half-life at the terminal phase of steady-state were 15.9 h and 38.4 h in the plasma and kidney, respectively. The difference in half-life could be linked to the higher exposure of enavogliflozin in the kidney (i.e., the target organ) than in the plasma. The AUC_{τ} for enavogliflozin in the kidney was predicted by the PBPK model as 100 ng·h/g tissue at the steady state after 0.3 mg once daily dosing of enavogliflozin in humans, and the total and unbound kidney-to-plasma partition coefficients for enavogliflozin (i.e., $K_{p,ss,KI,enavo}$ and $K_{p,uu,ss,KI,enavo}$, respectively) were predicted to be 2.67 and 8.49, respectively (Figure 6). The targeted exposure may be helpful in expanding the therapeutic window of enavogliflozin. Using the predicted unbound AUC in the kidney, the averaged unbound concentration of enavogliflozin at a steady state in the kidney ($C_{u,avg,ss,KI,enavo}$) was calculated after 0.3 mg/day oral dosing of enavogliflozin as 0.446 nmol/L (0.199 ng/mL), which was comparable to the reported IC_{50} in the previous SAR study (i.e., 0.46 nmol/L for SGLT2) [1]. Though the kidney model in this study could describe and predict in the expected range, there might be needs in the future to incorporate more mechanisms. For example, the kidney model in this study have multiple sub-compartments and physiological flows, but there are still missing physiologies, including bypass of blood flow and pH differences in the sub-compartments, which is included in the commercial model of Simcyp software (MechKiM) [50].

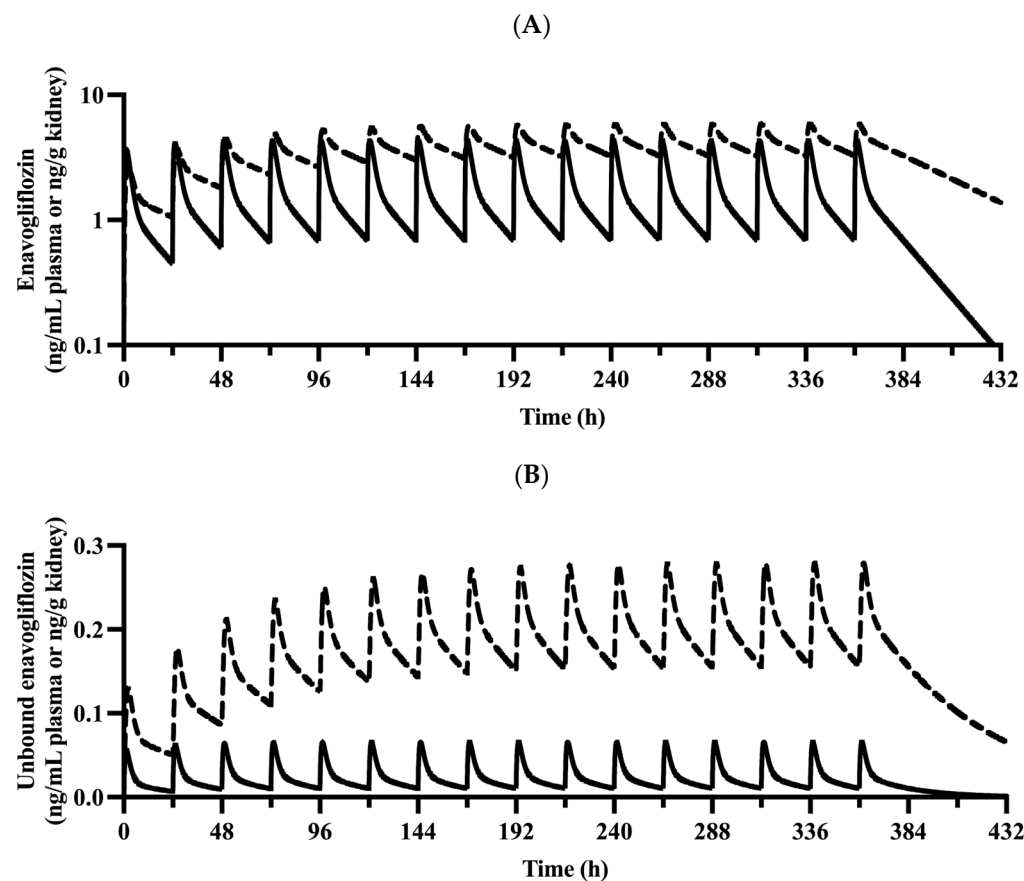


Figure 6. Predicted plasma and kidney total (A) and unbound (B) concentration profiles for enavogliflozin at repeated doses of 0.3 mg enavogliflozin administered to humans once daily for 15 days. Solid (—) and dashed (- -) lines represent the predicted concentration of enavogliflozin in the plasma and kidney, respectively.

PBPK modelling is useful in a predictive study, including first-in-human dose prediction, drug–drug interaction, pediatrics, geriatrics, altered physiologies, and different ethnicities [10–12,14,24]. As enavogliflozin is mainly eliminated by hepatic metabolism, the validated PBPK model for enavogliflozin was challenged in hepatic-impaired patients. Pathophysiological changes in the patients are described in the literature [12], and the fractional activities assumed for CYP2C19 were 0.5, 0.3, and 0.3 in the patients with Child–Pugh score A, B, and C, respectively, for the model of Andrea Edginton and Stefan Willmann [12,37]. Various isozymes are involved in the metabolism of enavogliflozin, including CYP3A4, CYP2C19, UGT1A4, UGT1A9, and UGT2B7 [8]. The primary metabolites of CYP3A4 and CYP2C19 pathways seemed to be M1 and M2, and the estimated contribution of CYP3A4 in the formation of M1 and M2 in this study was comparable to the reported results of anti-CYP3A4 antibody study in the literature [8]. The other primary metabolites were appeared to be generated by the other drug-metabolizing enzymes, such as UGT1A4, UGT1A9, and UGT2B7 [8]. Since UGTs were not reported as a consistent change in activities for the patients with hepatic impairment [37], the rest fraction, not metabolized to M1 and M2 (41.2%), was assumed not to be affected by the activity alteration of CYP3A4 and CYP2C19 but to be affected only by the changes in the active liver mass under the liver impairments.

Among the Child–Pugh classes, a PBPK model simulation was performed. AUC_{τ} for enavogliflozin in plasma was 45.3 ng·h/mL, 71.7 ng·h/mL, and 103 ng·h/mL, after orally administration of enavogliflozin 0.3 mg/day once daily in patients with Child–Pugh score of A, B, and C, respectively. The predicted AUC_{τ} for the patients with scores of A, B, and C were 121%, 191%, and 273%, respectively, compared with the prediction for healthy individuals. C_{max} were 3.76 ng/mL, 4.57 ng/mL, and 5.50 ng/mL in the patients with scores of A, B, and C, respectively, after the same dosing regimen. The predicted C_{max} values were 87.0%, 106%, and 127% compared with those predicted for healthy individuals. The predicted unbound fractions in plasma were 0.0187, 0.0222, and 0.0300 in the patients with the score A, B, and C, respectively, which were 123%, 146%, and 197% of the fraction in the plasma for healthy individuals. The predicted parameters for enavogliflozin were in the range from 80% to 125% range [51] for the patients with mild hepatic impairment (Child–Pugh score A), but the drug would have quite different pharmacokinetic characteristics in the patients with Child–Pugh scores B and C. Estimation for the M1, a major metabolite, concentration may be needed in the population for the further studies, such as dose adjustments.

5. Conclusions

In this study, PBPK models for enavogliflozin and M1 in humans were developed and evaluated using plasma concentration profiles from multiple clinical trials. For further study, a mechanistically arranged kidney model was developed, and the simulated unbound concentration of enavogliflozin in the kidney appeared to be relevant. The developed PBPK model may be useful for further pharmacokinetic and pharmacodynamic studies in humans.

Supplementary Materials: The following supporting information can be downloaded at: <https://www.mdpi.com/article/10.3390/pharmaceutics15030942/s1>, Table S1: Allometrically scaled effective surface area in humans; Table S2: Compartment volumes of the mechanistic kidney model; Table S3: Flow rates entering each compartment of the mechanistic kidney model. References [20,23,33–35] are cited in the supplementary materials.

Author Contributions: Conceptualization, M.-S.K., Y.-K.S., E.Y., S.-J.C. and K.-R.L.; Data curation, M.-S.K., Y.-K.S., J.-S.C., H.Y.J. and K.-R.L.; Formal analysis, M.-S.K., Y.-K.S., M.-J.K., I.-K.C. and K.-R.L.; Funding acquisition, K.-R.L.; Investigation, M.-S.K., Y.-K.S. and K.-R.L.; Methodology, M.-S.K., Y.-K.S., E.Y. and K.-R.L.; Project administration, J.-S.C., H.Y.J., J.S.P., H.S.K., S.-J.C. and K.-R.L.; Resources, J.-S.C., H.Y.J., E.Y., J.S.P., H.S.K., S.-J.C., Y.-J.C. and K.-R.L.; Software, M.-S.K., Y.-K.S. and K.-R.L.; Supervision, S.-J.C., Y.-J.C. and K.-R.L.; Validation, M.-S.K., Y.-K.S., J.S.P., H.S.K., Y.-J.C. and K.-R.L.; Visualization, M.-S.K., Y.-K.S. and K.-R.L.; Writing—original draft, M.-S.K., Y.-K.S. and K.-R.L.; Writing—review and editing, M.-S.K., Y.-K.S. and K.-R.L. All authors have read and agreed to the published version of the manuscript.

K.-R.L.; Writing—review & editing, M.-S.K., Y.-K.S., E.Y., J.S.P., H.S.K., Y.-J.C. and K.-R.L. All authors have read and agreed to the published version of the manuscript.

Funding: This research was supported by a grant from the KRIIB Research Initiative Program; the Technology Innovation Program (nos. 20009774) funded by the Ministry of Trade, Industry, and Energy (MOTIE, Korea); and the Basic Science Research Program through the National Research Foundation (NRF) of Korea funded by the Ministry of Education (2021R1I1A3056261).

Institutional Review Board Statement: Not applicable.

Informed Consent Statement: Not applicable.

Data Availability Statement: The cited clinical trial data were published by Hwang et al. (Clinical-Trials.gov: NCT03364985) [6].

Acknowledgments: This study was supported by Daewoong Pharmaceutical Co. Ltd., Seoul, Republic of Korea.

Conflicts of Interest: The authors declare no conflict of interest, but Ji-Soo Choi, Hye Young Ji and Joon Seok Park were employed by Daewoong Pharmaceuticals Co. Ltd. Data were acquired from clinical and/or non-clinical studies conducted or provided by Daewoong Pharmaceutical Co. Ltd. The data were reanalyzed by the authors. The company had no role in the data analysis or interpretation, manuscript writing, or publication of the results.

Appendix A Kidney Sub-Compartments for Enavogliflozin

Appendix A.1 Blood Compartments

In blood compartments, changes in drug concentrations are driven by blood flow through the segments and passive transport to the cellular compartments. For proximal tubular blood compartments, active transport to cellular compartments (i.e., secretion) was also incorporated.

Differential equations for enavogliflozin in the blood compartments were:

1. Glomerular Blood (i.e., Bowman's Capsule)

$$\frac{d(C_{bcvas})}{dt} = (Q_{kid} \cdot C_{ar} - (Q_{kid} - GFR) \cdot C_{bcvas} - GFR \cdot f_{ub} \cdot C_{bcvas}) / V_{bcvas} \quad (\text{A1})$$

2. Proximal Tubular Blood

$$\frac{d(C_{ptvas,i})}{dt} = \{(Q_{kid} - GFR) \cdot C_{bcvas} - (Q_{kid} - Q_{ptlum,i+1}) \cdot C_{ptvas,i} - CL_{sec} \cdot C_{ptvas,i} \cdot f_{ub} + P_{pd} \cdot SA_{pt,i} \cdot (C_{ptc,i} \cdot f_{ucell} - C_{ptvas,i} \cdot f_{ub})\} / V_{ptvas,i} \quad (\text{A2})$$

where i refers to the subsection of the proximal tubule from 1 to 3. For $i = 2$ or 3, $(Q_{kid} - Q_{ptlum,i}) \cdot C_{ptvas,i-1}$ was used instead of $(Q_{kid} - GFR) \cdot C_{bcvas}$.

3. Blood at the Loop of Henle

$$\frac{d(C_{lhvas})}{dt} = \{(Q_{kid} - Q_{lhlu}) \cdot C_{ptvas,3} - (Q_{kid} - Q_{dtlum}) \cdot C_{lhvas} + P_{pd} \cdot SA_{lh} \cdot (C_{lhc} \cdot f_{ucell} - C_{lhvas} \cdot f_{ub})\} / V_{lhvas} \quad (\text{A3})$$

4. Blood at the Distal tubule

$$\frac{d(C_{dtvas})}{dt} = \{(Q_{kid} - Q_{dtlum}) \cdot C_{lhvas} - (Q_{kid} - Q_{cdlum,1}) \cdot C_{dtvas} + P_{pd} \cdot SA_{dt} \cdot (C_{dtc} \cdot f_{u,cell} - C_{dtvas} \cdot f_{ub})\} / V_{dtvas} \quad (\text{A4})$$

5. Blood at the Collecting Duct

$$\frac{d(C_{cdvas,i})}{dt} = \{(Q_{kid} - Q_{cdlum,i}) \cdot C_{dtvas} - (Q_{kid} - Q_{cdlum,i+1}) \cdot C_{cdvas,i} + P_{pb} \cdot SA_{cd,i} \cdot (C_{cdc,i} \cdot f_{u,cell} - C_{cdvas,i} \cdot f_{ub})\} / V_{cdvas,i} \quad (\text{A5})$$

where i refers to the subsection of the collecting duct from 1 to 2. For $i = 2$, $(Q_{\text{kid}} - Q_{\text{cdlum},i})$ was multiplied with $C_{\text{cdvas},i-1}$, and $C_{\text{cdvas},i}$ was multiplied with $(Q_{\text{kid}} - Q_{\text{urine}})$ instead of $(Q_{\text{kid}} - Q_{\text{cdlum},i+1})$.

Appendix A.2 Cellular Compartments

In cellular compartments, the change in drug concentrations are driven by passive diffusion between the vascular compartment and the cells and cells and luminal compartments. For proximal tubular blood compartments, active transport from cellular (i.e., secretion) and luminal (i.e., reabsorption) compartments were also incorporated.

Differential equations for enavoglitazin in the cellular compartments were:

6. Cellular Compartments at the Proximal Tubule

$$\frac{d(C_{\text{ptc},i})}{dt} = \{ CL_{\text{sec}} \cdot C_{\text{ptvas},i} \cdot f_{ub} + P_{pd} \cdot SA_{\text{pt},i} \cdot (C_{\text{ptvas},i} \cdot f_{ub} - C_{\text{ptc},i} \cdot f_{u,cell}) + V_{\text{max},\text{reab}} \cdot (K_m,\text{reab} + C_{\text{ptlum},i}) \cdot C_{\text{ptlum},i} \cdot P_{pd} \cdot SA_{\text{pt},i} \cdot (C_{\text{ptlum},i} - C_{\text{ptc},i} \cdot f_{u,cell}) \} / V_{\text{ptc},i} \quad (\text{A6})$$

7. The Cellular Compartment at Loop of Henle

$$\frac{d(C_{\text{lhc}})}{dt} = \{ P_{pd} \cdot SA_{\text{lh}} \cdot (C_{\text{lhvas}} \cdot f_{ub} - C_{\text{lhc}} \cdot f_{u,cell}) + P_{pd} \cdot SA_{\text{lh}} \cdot (C_{\text{lhlum}} - C_{\text{lhc}} \cdot f_{u,cell}) \} / V_{\text{lhc}} \quad (\text{A7})$$

8. Cellular Compartments at the Distal Tubule

$$\frac{d(C_{\text{dtc}})}{dt} = \{ P_{pd} \cdot SA_{\text{dt}} \cdot (C_{\text{dtvas}} \cdot f_{ub} - C_{\text{dtc}} \cdot f_{u,cell}) + P_{pd} \cdot SA_{\text{dt}} \cdot (C_{\text{dtlum}} - C_{\text{dtc}} \cdot f_{u,cell}) \} / V_{\text{dtc}} \quad (\text{A8})$$

9. Cellular Compartments at the Collecting Duct

$$\frac{d(C_{\text{cdc},i})}{dt} = \{ P_{pb} \cdot SA_{\text{cd},i} \cdot (C_{\text{cdvas}} \cdot f_{ub} - C_{\text{cdc},i} \cdot f_{u,cell}) + P_{pd} \cdot SA_{\text{cd},i} \cdot (C_{\text{cdlum},i} - C_{\text{cdc},i} \cdot f_{u,cell}) \} / V_{\text{cdc},i} \quad (\text{A9})$$

Appendix A.3 Luminal Compartments

The urine filtrate was assumed to flow through the kidney lumen. Differential equations for enavoglitazin in the luminal compartments were as follows:

10. Glomerular Space (i.e., Bowman's Capsule)

$$\frac{d(C_{\text{bclum}})}{dt} = (GFR \cdot f_{ub} \cdot C_{\text{bcvas}} - Q_{\text{ptlum}1} \cdot C_{\text{bclum}}) / V_{\text{bclum}} \quad (\text{A10})$$

11. Lumen of Proximal Tubule

$$\frac{d(C_{\text{ptlum},i})}{dt} = \{ Q_{\text{ptlum},i} \cdot C_{\text{bclum}} - Q_{\text{ptlum},i+1} \cdot C_{\text{ptlum},i} - V_{\text{max},\text{reab}} \cdot (K_m,\text{reab} + C_{\text{ptlum},i}) \cdot C_{\text{ptlum},i} + P_{pd} \cdot SA_{\text{pt},i} \cdot (C_{\text{ptc},i} \cdot f_{u,cell} - C_{\text{ptlum},i}) \} / V_{\text{ptlum},i} \quad (\text{A11})$$

where i refers to the subsection of the proximal tubule from 1 to 3. For $i = 2$ or 3, $Q_{\text{ptlum},i}$ was multiplied with $C_{\text{ptlum},i-1}$ instead of C_{bclum} .

12. Lumen at the Loop of Henle

$$\frac{d(C_{\text{lhlum}})}{dt} = \{ Q_{\text{lhlum}} \cdot C_{\text{ptlum},3} - Q_{\text{dtlum}} \cdot C_{\text{lhlum}} + P_{pd} \cdot SA_{\text{lh}} \cdot (C_{\text{lhc}} \cdot f_{u,cell} - C_{\text{lhlum}}) \} / V_{\text{lhlum}} \quad (\text{A12})$$

13. Lumen at the Distal Tubule

$$\frac{d(C_{\text{dtlum}})}{dt} = \{ Q_{\text{dtlum}} \cdot C_{\text{lhlum}} - Q_{\text{cdlum}} \cdot C_{\text{dtlum}} + P_{pd} \cdot SA_{\text{dt}} \cdot (C_{\text{dtc}} \cdot f_{u,cell} - C_{\text{dtlum}}) \} / V_{\text{dtlum}} \quad (\text{A13})$$

14. Lumen at the Collecting Duct

$$\frac{d(C_{cdlum,i})}{dt} = \left\{ Q_{cdlum,i} C_{dtlum} - Q_{cdlum,i+1} C_{cdlum,i} + P_{pd} \cdot S A_{cd,i} \cdot (C_{cdc,i} f_{u,cell} - C_{cdlum,i}) \right\} / V_{cdlum,i} \quad (\text{A14})$$

where i refers to the subsection of the collecting duct from 1 to 2. For $i = 2$, $Q_{cdlum,i}$ was multiplied with $C_{cdlum,i-1}$ instead of C_{dtlum} . $Q_{cdlum,3}$ was substituted by Q_{urine} .

References

- Kong, Y.K.; Song, K.-S.; Jung, M.E.; Kang, M.; Kim, H.J.; Kim, M.J. Discovery of GCC5694A: A Potent and Selective Sodium Glucose Co-transporter 2 Inhibitor for the Treatment of Type 2 Diabetes. *Bioorg. Med. Chem. Lett.* **2022**, *56*, 128466. [\[CrossRef\]](#)
- Poulsen, S.B.; Fenton, R.A.; Rieg, T. Sodium-Glucose Cotransport. *Curr. Opin. Nephrol. Hypertens.* **2015**, *24*, 463–469. [\[CrossRef\]](#)
- Vallon, V.; Platt, K.A.; Cunard, R.; Schroth, J.; Whaley, J.; Thomson, S.C.; Koepsell, H.; Rieg, T. SGLT2 Mediates Glucose Reabsorption in the Early Proximal Tubule. *J. Am. Soc. Nephrol.* **2011**, *22*, 104–112. [\[CrossRef\]](#) [\[PubMed\]](#)
- Wright, E.M. Renal Na⁺-Glucose Cotransporters. *Am. J. Physiol.-Ren. Physiol.* **2001**, *280*, F10–F18. [\[CrossRef\]](#)
- Daewoong Pharmaceutical Co., Ltd. *Daewoong Pharmaceutical Announces Success in Developing a New Antidiabetic Medication and Its Aims to Enter the Market in over 50 Countries by 2030*; Daewoong Pharmaceutical Co., Ltd.: Seoul, Republic of Korea, 2022.
- Hwang, J.; Lee, S.; Huh, W.; Han, J.; Oh, J.; Jang, I.-J.; Yu, K.-S. Dose-Dependent Glucosuria of DWP16001, a Novel Selective SGLT-2 Inhibitor, in Healthy Subjects. *Br. J. Clin. Pharmacol.* **2022**, *88*, 4100–4110. [\[CrossRef\]](#)
- U.S. Food and Drug Administration (US FDA). *Safety Testing of Drug Metabolites—Guidance for Industry*; U.S. Food and Drug Administration (US FDA): Silver Spring, MD, USA, 2020.
- Kim, J.H.; Kim, D.K.; Choi, W.G.; Ji, H.Y.; Choi, J.S.; Song, I.S.; Lee, S.; Lee, H.S. In Vitro Metabolism of DWP16001, a Novel Sodium-Glucose Cotransporter 2 Inhibitor, in Human and Animal Hepatocytes. *Pharmaceutics* **2020**, *12*, 865. [\[CrossRef\]](#)
- Plum, A.; Jensen, L.B.; Kristensen, J.B. In Vitro Protein Binding of Liraglutide in Human Plasma Determined by Reiterated Stepwise Equilibrium Dialysis. *J. Pharm. Sci.* **2013**, *102*, 2882–2888. [\[CrossRef\]](#) [\[PubMed\]](#)
- Yim, C.-S.; Jeong, Y.-S.; Lee, S.-Y.; Pyeon, W.; Ryu, H.-M.; Lee, J.-H.; Lee, K.-R.; Maeng, H.-J.; Chung, S.-J. Specific Inhibition of the Distribution of Lobeglitazone to the Liver by Atorvastatin in Rats: Evidence for a Rat Organic Anion Transporting Polypeptide 1B2-Mediated Interaction in Hepatic Transport. *Drug Metab. Dispos.* **2017**, *45*, 246–259. [\[CrossRef\]](#) [\[PubMed\]](#)
- Jamei, M.; Marciak, S.; Feng, K.; Barnett, A.; Tucker, G.; Rostami-Hodjegan, A. The Simcyp® Population-Based ADME Simulator. *Expert Opin. Drug Metab. Toxicol.* **2009**, *5*, 211–223. [\[CrossRef\]](#)
- Edginton, A.N.; Willmann, S. Physiology-Based Simulations of a Pathological Condition. *Clin. Pharmacokinet.* **2008**, *47*, 743–752. [\[CrossRef\]](#)
- Jeong, Y.-S.; Kim, M.-S.; Lee, N.; Lee, A.; Chae, Y.-J.; Chung, S.-J.; Lee, K.-R. Development of Physiologically Based Pharmacokinetic Model for Orally Administered Fexuprazaran in Humans. *Pharmaceutics* **2021**, *13*, 813. [\[CrossRef\]](#)
- Malik, P.R.V.; Yeung, C.H.T.; Ismaeil, S.; Advani, U.; Djie, S.; Edginton, A.N. A Physiological Approach to Pharmacokinetics in Chronic Kidney Disease. *J. Clin. Pharmacol.* **2020**, *60*, S52–S62. [\[CrossRef\]](#)
- Davies, B.; Morris, T. Physiological Parameters in Laboratory Animals and Humans. *Pharm. Res.* **1993**, *10*, 1093–1095. [\[CrossRef\]](#) [\[PubMed\]](#)
- Brown, R.P.; Delp, M.D.; Lindstedt, S.L.; Rhomberg, L.R.; Beliles, R.P. Physiological Parameter Values for Physiologically Based Pharmacokinetic Models. *Toxicol. Ind. Health* **1997**, *13*, 407–484. [\[CrossRef\]](#)
- Sun, D.; Lennernas, H.; Welage, L.S.; Barnett, J.L.; Landowski, C.P.; Foster, D.; Fleisher, D.; Lee, K.-D.; Amidon, G.L. Comparison of Human Duodenum and Caco-2 Gene Expression Profiles for 12,000 Gene Sequences Tags and Correlation with Permeability of 26 Drugs. *Pharm. Res.* **2002**, *19*, 1400–1416. [\[CrossRef\]](#) [\[PubMed\]](#)
- Lennernas, H. Intestinal Permeability and Its Relevance for Absorption and Elimination. *Xenobiotica* **2007**, *37*, 1015–1051. [\[CrossRef\]](#) [\[PubMed\]](#)
- Jeong, Y.-S.; Jusko, W.J. Consideration of Fractional Distribution Parameter fd in the Chen and Gross Method for Tissue-to-Plasma Partition Coefficients: Comparison of Several Methods. *Pharm. Res.* **2022**, *39*, 463–479. [\[CrossRef\]](#) [\[PubMed\]](#)
- Jeong, Y.-S.; Yim, C.-S.; Ryu, H.-M.; Noh, C.-K.; Song, Y.-K.; Chung, S.-J. Estimation of the Minimum Permeability Coefficient in Rats for Perfusion-Limited Tissue Distribution in Whole-Body Physiologically-Based Pharmacokinetics. *Eur. J. Pharm. Biopharm.* **2017**, *115*, 1–17. [\[CrossRef\]](#)
- Yamazaki, M.; Akiyama, S.; Nishigaki, R.; Sugiyama, Y. Uptake Is the Rate-limiting Step in the Overall Hepatic Elimination of Pravastatin at Steady-state in Rats. *Pharm. Res.* **1996**, *13*, 1559–1564. [\[CrossRef\]](#)
- Jeong, Y.-S.; Kim, M.-S.; Chung, S.-J. Determination of the Number of Tissue Groups of Kinetically Distinct Transit Time in Whole-Body Physiologically Based Pharmacokinetic (PBPK) Models II: Practical Application of Tissue Lumping Theories for Pharmacokinetics of Various Compounds. *AAPS J.* **2022**, *24*, 91. [\[CrossRef\]](#)
- Shin, J.-W.; Seol, I.-C.; Son, C.-G. Interpretation of Animal Dose and Human Equivalent Dose for Drug Development. *J. Korean Med.* **2010**, *31*, 1–7.
- Barter, Z.E.; Chowdry, J.E.; Harlow, J.R.; Snawder, J.E.; Lipscomb, J.C.; Rostami-Hodjegan, A. Covariation of Human Microsomal Protein per Gram of Liver with Age: Absence of Influence of Operator and Sample Storage May Justify Interlaboratory Data Pooling. *Drug Metab. Dispos.* **2008**, *36*, 2405–2409. [\[CrossRef\]](#) [\[PubMed\]](#)

25. Rodgers, T.; Rowland, M. Physiologically Based Pharmacokinetic Modelling 2: Predicting the Tissue Distribution of Acids, Very Weak Bases, Neutrals and Zwitterions. *J. Pharm. Sci.* **2006**, *95*, 1238–1257. [[CrossRef](#)]
26. Rodgers, T.; Rowland, M. Mechanistic Approaches to Volume of Distribution Predictions: Understanding the Processes. *Pharm. Res.* **2007**, *24*, 918–933. [[CrossRef](#)]
27. Øie, S.; Tozer, T.N. Effect of Altered Plasma Protein Binding on Apparent Volume of Distribution. *J. Pharm. Sci.* **1979**, *68*, 1203–1205. [[CrossRef](#)]
28. Poulin, P.; Theil, F.P. Prediction of Pharmacokinetics Prior to In Vivo Studies. 1. Mechanism-Based Prediction of Volume of Distribution. *J. Pharm. Sci.* **2002**, *91*, 129–156. [[CrossRef](#)]
29. Watanabe, R.; Esaki, T.; Kawashima, H.; Natsume-Kitatani, Y.; Nagao, C.; Ohashi, R.; Mizuguchi, K. Predicting Fraction Unbound in Human Plasma from Chemical Structure: Improved Accuracy in the Low Value Ranges. *Mol. Pharm.* **2018**, *15*, 5302–5311. [[CrossRef](#)] [[PubMed](#)]
30. Rodgers, T.; Leahy, D.; Rowland, M. Physiologically Based Pharmacokinetic Modeling 1: Predicting the Tissue Distribution of Moderate-To-Strong Bases. *J. Pharm. Sci.* **2005**, *94*, 1259–1276. [[CrossRef](#)]
31. Pfeifer, N.D.; Harris, K.B.; Yan, G.Z.; Brouwer, K.L.R. Determination of Intracellular Unbound Concentrations and Subcellular Localization of Drugs in Rat Sandwich-Cultured Hepatocytes Compared with Liver Tissue. *Drug Metab. Dispos.* **2013**, *41*, 1949. [[CrossRef](#)] [[PubMed](#)]
32. Kalvass, J.C.; Maurer, T.S.; Pollack, G.M. Use of Plasma and Brain Unbound Fractions to Assess the Extent of Brain Distribution of 34 Drugs: Comparison of Unbound Concentration Ratios to in Vivo P-Glycoprotein Efflux Ratios. *Drug Metab. Dispos.* **2007**, *35*, 660. [[CrossRef](#)]
33. Pletz, J.; Allen, T.J.; Madden, J.C.; Cronin, M.T.D.; Webb, S.D. A Mechanistic Model to Study the Kinetics and Toxicity of Salicylic Acid in the Kidney of Four Virtual Individuals. *Comput. Toxicol.* **2021**, *19*, 100172. [[CrossRef](#)]
34. Scotcher, D.; Jones, C.; Posada, M.; Rostami-Hodjegan, A.; Galetin, A. Key to Opening Kidney for In Vitro–In Vivo Extrapolation Entrance in Health and Disease: Part I: In Vitro Systems and Physiological Data. *AAPS J.* **2016**, *18*, 1067–1081. [[CrossRef](#)]
35. Scotcher, D.; Jones, C.; Posada, M.; Galetin, A.; Rostami-Hodjegan, A. Key to Opening Kidney for In Vitro–In Vivo Extrapolation Entrance in Health and Disease: Part II: Mechanistic Models and In Vitro–In Vivo Extrapolation. *AAPS J.* **2016**, *18*, 1082–1094. [[CrossRef](#)] [[PubMed](#)]
36. Chen, Y.; Liu, L.; Nguyen, K.; Fretland, A.J. Utility of Intersystem Extrapolation Factors in Early Reaction Phenotyping and the Quantitative Extrapolation of Human Liver Microsomal Intrinsic Clearance Using Recombinant Cytochromes P450. *Drug Metab. Dispos.* **2011**, *39*, 373. [[CrossRef](#)] [[PubMed](#)]
37. Johnson, T.N.; Boussey, K.; Rowland-Yeo, K.; Tucker, G.T.; Rostami-Hodjegan, A. A Semi-Mechanistic Model to Predict the Effects of Liver Cirrhosis on Drug Clearance. *Clin. Pharmacokinet.* **2010**, *49*, 189–206. [[CrossRef](#)]
38. Esaki, T.; Watanabe, R.; Kawashima, H.; Ohashi, R.; Natsume-Kitatani, Y.; Nagao, C.; Mizuguchi, K. Data Curation can Improve the Prediction Accuracy of Metabolic Intrinsic Clearance. *Mol. Inform.* **2019**, *38*, 1800086. [[CrossRef](#)]
39. Watanabe, R.; Ohashi, R.; Esaki, T.; Kawashima, H.; Natsume-Kitatani, Y.; Nagao, C.; Mizuguchi, K. Development of an in Silico Prediction System of Human Renal Excretion and Clearance from Chemical Structure Information Incorporating Fraction Unbound in Plasma as a Descriptor. *Sci. Rep.* **2019**, *9*, 18782. [[CrossRef](#)]
40. Choi, M.-K.; Nam, S.J.; Ji, H.-Y.; Park, M.J.; Choi, J.-S.; Song, I.-S. Comparative Pharmacokinetics and Pharmacodynamics of a Novel Sodium-Glucose Cotransporter 2 Inhibitor, DWP16001, with Dapagliflozin and Ipragliflozin. *Pharmaceutics* **2020**, *12*, 268. [[CrossRef](#)]
41. Kasichayanula, S.; Liu, X.; Zhang, W.; Pfister, M.; LaCreta, F.P.; Boulton, D.W. Influence of Hepatic Impairment on the Pharmacokinetics and Safety Profile of Dapagliflozin: An Open-Label, Parallel-Group, Single-Dose Study. *Clin. Ther.* **2011**, *33*, 1798–1808. [[CrossRef](#)]
42. Sung, S.; Al-Karaghoubi, M.; Kalainy, S.; Cabrera Garcia, L.; Abraldes, J.G. A Systematic Review on Pharmacokinetics, Cardiovascular Outcomes and Safety Profiles of Statins in Cirrhosis. *BMC Gastroenterol.* **2021**, *21*, 120. [[CrossRef](#)]
43. Kim, C.O.; Jeon, S.; Han, S.; Hong, T.; Park, M.S.; Yoon, Y.-R.; Yim, D.-S. Decreased Potency of Fimasartan in Liver Cirrhosis Was Quantified Using Mixed-Effects Analysis. *Transl. Clin. Pharmacol.* **2017**, *25*, 43–51. [[CrossRef](#)]
44. Pang, M.; Jeon, S.Y.; Choi, M.-K.; Jeon, J.-H.; Ji, H.-Y.; Choi, J.-S.; Song, I.-S. Pharmacokinetics and Tissue Distribution of Enavogliflozin in Mice and Rats. *Pharmaceutics* **2022**, *14*, 1210. [[CrossRef](#)]
45. Yu, L.X.; Amidon, G.L. A Compartmental Absorption and Transit Model for Estimating Oral Drug Absorption. *Int. J. Pharm.* **1999**, *186*, 119–125. [[CrossRef](#)] [[PubMed](#)]
46. Huang, W.; Lee, S.I.; Yu, L.X. Mechanistic Approaches to Predicting Oral Drug Absorption. *AAPS J.* **2009**, *11*, 217–224. [[CrossRef](#)] [[PubMed](#)]
47. Thelen, K.; Coboeken, K.; Willmann, S.; Burghaus, R.; Dressman, J.B.; Lippert, J. Evolution of a Detailed Physiological Model to Simulate the Gastrointestinal Transit and Absorption Process in Humans, Part 1: Oral Solutions. *J. Pharm. Sci.* **2011**, *100*, 5324–5345. [[CrossRef](#)] [[PubMed](#)]
48. Thelen, K.; Coboeken, K.; Willmann, S.; Dressman, J.B.; Lippert, J. Evolution of a Detailed Physiological Model to Simulate the Gastrointestinal Transit and Absorption Process in Humans, Part II: Extension to Describe Performance of Solid Dosage Forms. *J. Pharm. Sci.* **2012**, *101*, 1267–1280. [[CrossRef](#)]

49. Fagerholm, U. Prediction of Human Pharmacokinetics—Renal Metabolic and Excretion Clearance. *J. Pharm. Pharmacol.* **2007**, *59*, 1463–1471. [[CrossRef](#)] [[PubMed](#)]
50. Neuhoff, S.; Gaohua, L.; Burt, H.; Jamei, M.; Li, L.; Tucker, G.T.; Rostami-Hodjegan, A. Accounting for Transporters in Renal Clearance: Towards a Mechanistic Kidney Model (Mech KiM). In *Transporters in Drug Development: Discovery, Optimization, Clinical Study and Regulation*; Sugiyama, Y., Steffansen, B., Eds.; Springer: New York, NY, USA, 2013; pp. 155–177.
51. U.S. Food and Drug Administration (US FDA). *Pharmacokinetics in Patients with Impaired Hepatic Function: Study Design, Data Analysis, and Impact on Dosing and Labeling—Guidance for Industry*; U.S. Food and Drug Administration (US FDA): Silver Spring, MD, USA, 2003.

Disclaimer/Publisher’s Note: The statements, opinions and data contained in all publications are solely those of the individual author(s) and contributor(s) and not of MDPI and/or the editor(s). MDPI and/or the editor(s) disclaim responsibility for any injury to people or property resulting from any ideas, methods, instructions or products referred to in the content.